Carbon 213 (2023) 118229

Contents lists available at ScienceDirect

Carbon

journal homepage: www.elsevier.com/locate/carbon

Long-term antibacterial activity of guanidinium carbon dots without detectable resistance for the effective treatment of pneumonia caused by Gram-negative bacteria

Xintian Zhang [a,1], XinXin Bai [d,1], Xiaoqin Deng [a], Kai Peng [b], Zongfu Zheng [b], Jiecheng Xiao [d], Rui Zhang [d], Zhengjun Huang [a], Jianyong Huang [c,***], Min Chen [d,**], Shaohuang Weng [a,*]

[a] Department of Pharmaceutical Analysis, School of Pharmacy, Fujian Medical University, Fuzhou, 350122, China
[b] Cangshan Campus of the 900th Hospital of Joint Logistics Team of the PLA, Fuzhou General Clinical Medical College of Fujian Medical University, Fuzhou, 350002, China
[c] Department of Pharmacy, Fujian Medical University Union Hospital, Fuzhou, 350001, China
[d] Department of Orthopedic Surgery, Fujian Medical University Union Hospital, Fuzhou, 350001, China

ARTICLE INFO

Keywords:
Guanidinium carbon dots
Gram-negative bacteria
Long-term stability
No resistance development
Infected pneumonia
Intravenous therapy

ABSTRACT

The development of nanomedicine for the treatment of infection caused by resistant bacteria, especially Gram-negative bacteria, is still in the bottleneck. The long-term antibacterial activity and the low induced resistance risk need improvement. Herein, guanidinium-based carbon dots (G-CDs) were prepared from citric acid, dimethyldiallylammonium chloride, and polyhexamethyleneguanidine through melting strategy. The antibacterial properties of G-CDs against Gram-negative and resistant bacteria were investigated. G-CDs exhibit strong and long-term antibacterial activity, as well as antibiofilm activity, with less potential for inducing bacterial resistance. The antibacterial mechanism of G-CDs of the adsorption action and killing effect was elucidated, which was different from the mechanism of antibiotics. Moreover, derived from the interacting mode of nanomaterials and ssDNA, the enhanced ability of G-CDs against Gram-negative bacteria was studied based on the found interaction of G-CDs and lipopolysaccharide (LPS) for the understanding of the mode for the absorption of G-CDs on the cell wall of Gram-negative bacteria. The multimode interactions of van der Waals force, electrostatic adsorption and hydrogen bonding were clarified. Furthermore, G-CDs had excellent *in vivo* safety and *in vivo* therapeutic effects in *E. coli*-infected pneumonia through an intravenous approach. This study provides a hopeful strategy for developing antibacterial drugs from understanding the interacting mode of the drug and the cell wall of bacteria.

1. Introduction

As COVID-19 rages on, the pandemic of antimicrobial resistance (AMR) continues in the shadows [1]. AMR, which mainly occurs when bacterial changes caused by the misuse and/or overuse of antibiotics, results in a dramatic decrease in antibiotic effectiveness. The global threat posed by AMR is acknowledged by the World Health Organization (WHO) and the U.S. Centers for Disease Control and Prevention (CDC) [2]. If left unchecked, the spread of AMR may induce more lethal bacterial pathogens in the future. Against this background, in 2018, the WHO published a list of priority pathogens that are resistant to antibiotics, most of which are Gram-negative (G^-) bacteria [3]. Due to their unique shielded structure by the outer membrane, most notably the composition of lipopolysaccharide (LPS) [4–6], G^- bacteria are more susceptible to drug resistance than Gram-positive (G^+) bacteria and cause severe morbidity and mortality worldwide [7]. In populations with weakened or underdeveloped immune systems, G^- bacteria can result in serious and fatal infections, such as the hospital-acquired pneumonia (HAP), urinary tract infections, and sepsis [8]. Currently, infections caused by G^- bacteria have become one of the most

* Corresponding author.
** Corresponding author.
*** Corresponding author.
E-mail addresses: hjy8191@163.com (J. Huang), chenminfz006@163.com (M. Chen), shweng@fjmu.edu.cn (S. Weng).
[1] Zhang and Bai contributed equally to this work.

https://doi.org/10.1016/j.carbon.2023.118229
Received 29 March 2023; Received in revised form 19 June 2023; Accepted 19 June 2023
Available online 20 June 2023

challenging problems in clinical practice. Relatively, the pathogens of HAP are prone to develop into drug-resistance G^- bacteria. In recent years, chemical synthesis, exploitation of new kinds of antibiotic and peptide synthesis have been developed to be potential antibacterial drugs [9–12]. The exploration of alternative strategies for G^+ bacteria has achieved a gratifying posture [13–16]. Unfortunately, there is still a paucity of alternative new therapeutic solutions that are effective against G^- and drug-resistant bacteria. Most of the recently developed antimicrobial drugs available exert their antimicrobial action mainly through mechanisms similar to those of conventional antibiotics, leaving the incidence of bacterial resistance unchecked. The lack of effective antibiotics in reserve and the existence of irrational use of drugs warn us that the development of new antibacterial approaches is urgent and critical, especially for the weapon against G^- bacteria.

In the past decade, the rapid development of nanotechnology has provided promising options for antimicrobial strategies. Recently, different kinds of nanomaterials for medicine, including polymeric nanoparticles, metallic nanoparticles, metal oxides, and carbon nanomaterials, have been designed and applied as bactericidal/bacteriostatic agents [17–19]. Furthermore, active nanoparticles can also be hoped to treat biofilm-associated infections through the fabrication of approaches with enhanced permeability to matrix barriers [20,21]. Carbon dots, zero-dimensional carbon-based fluorescent nanomaterial, have attracted increased attention in the biomedical fields because of their excellent optical properties, biocompatibility, and adjustable bioactivities [22–26]. Carbon dots can be optimized by the design of synthetic methods and raw materials as well as the modification of hetero-elemental doping and functional groups from source molecules to achieve the modulation of the core structure and surface properties for biomedical applications with specific target requirements. In recent studies, several antimicrobial carbon dots, such as folic acid-derived carbon dots (FA-CDs) [27], copper-doped carbon dots [28], nitrogen-doped carbon quantum dots (NCQDs) [29], and quaternized carbon dots [30], have been prepared using bottom-up strategies and been developed to combat bacteria through a specific absorption behavior and further killing effect after penetration.

In general, most of the antimicrobial carbon dots exhibit considerable activity against G^+ bacteria and good therapeutic effect on G^+ bacteria-infected wounds [27,29,31,32]. The antimicrobial properties of carbon dots on G^- bacteria are barely satisfactory [27,33,34]. The main reason for the current antibacterial carbon dots with enhanced ability to G^+ bacteria may be that the currently antimicrobial carbon dots acting on bacteria is mainly through electrostatic or hydrophobic adsorption on the bacterial surface with the following entry and the production of antibacterial components (like reactive oxygen species, ROS) [35]. However, ascribed to the protective effect of the outer membrane of G^- bacteria, the electrostatic interaction or only one action may be weakened on the cell wall of G^- bacteria [36]. A smaller number of active nanoparticles can penetrate this barrier, and combat G^- bacteria. Therefore, the hypothesis of the development of effective carbon dots that enhance the absorption with bacteria, particularly G^- bacteria, with specific components of the cell wall is expected to improve their activity against G^- bacteria. In addition, it is known that the long-term stability of the efficacy of nanomedicine is a significant aspect that affects the ultimate clinical application prospect. However, the long-term stability of many reported antimicrobial carbon dots or nanomaterials is still unclear or has not investigated. Currently, the *in vivo* models of antimicrobial carbon dots are mainly applied as external medicine through administration approaches of coating or dropping [37,38]. Injection therapy, especially for intravenous approaches, is the most important and predominant mode of drug delivery in clinical and medical practice. Yet it remains an open question as to whether injectable therapies are effective modes of carbon dots in the intervention of bacterial infection models.

The carbon dots prepared from bottom-up strategies using small molecules can help the carbon dots retain the original functional groups of the introduced raw molecules, which are effective approaches to produce carbon dots with some activities [39]. Citric acid is one of the main raw molecules for the formation of carbon nucleus through bottom-up synthetic strategies [40]. Quaternary ammonium compounds and guanidine compounds have long chain groups, positive charges and the nitrogen sources for doping. As raw materials, the quaternary ammonium, guanidine, and long chain groups are expected to be kept in the prepared carbon dots, which may promote the interaction between carbon dots and bacteria due to the retention groups [41,42]. In this study, we have designed and synthesized the broad-spectrum antibacterial guanidinium carbon dots (G-CDs) based on the clinical concerns of antibacterial drugs of long-term stable activity and none detectable resistance (Scheme 1). G-CDs are prepared from citric acid, quaternary ammonium compounds (dimethyldiallylammonium chloride, DDA) and guanidine compounds (polyhexamethyleneguanidine, PHMG) by melting method. The antimicrobial performance studies exhibit that G-CDs have powerful activity against G^- bacteria, clinically resistant bacteria, and have anti-biofilm activity. At the same time, G-CDs show stable antibacterial properties even after long-term storage. In addition, studies on the antibacterial mechanism of G-CDs suggest that G-CDs enhance adsorption on the surface of G^- bacteria through van der Waals (vdW) forces, electrostatic attraction, and hydrogen bonding, thus leading to bacterial death by disrupting bacterial cell membranes, producing ROS and binding bacterial DNA. More importantly, unlike the problem of bacterial resistance due to the long-term migration of conventional antibiotics, since G-CDs can inhibit the activity of the bacterial efflux pump by suppressing bacterial ATP levels, G-CDs fight drug-resistant bacteria without causing new resistance. Systematic studies of the biosafety of G-CDs *in vitro* and *in vivo* confirm that G-CDs are generally safe for antimicrobial use. In further, intravenous administration of G-CDs also exhibits excellent *in vivo* therapeutic efficacy against *E. coli*-infected pneumonia. Overall, the availability of such stable G-CDs with excellent antimicrobial properties, the in-depth study of antimicrobial mechanisms, and the attempt to use injection therapy for *in vivo* interventions, establish a vision for the development of carbon dots to achieve clinical application prospects in the antimicrobial field.

2. Experimental part

2.1. Reagents and apparatus

Anhydrous citric acid (CA), dimethyldiallylammonium chloride (DDA), and 2′,7′-dichlorodihydrofluorescein diacetate (DCFH-DA) were purchased from Shanghai Aladdin Bio-chem Technology Co., LTD (China). Polyhexamethyleneguanidine hydrochloride (PHMG), levofloxacin, and glacial acetic acid were purchased from Shanghai Macklin Biochemical CO., LTD (China). Mueller-Hinton (MH) broth and nutrient agar (NA) were purchased from Qingdao Hi-tech Industrial Park Hope Bio-technology Co., LTD (China). Fetal bovine serum was purchased from Gibco Life Technologies (USA). Rabbit serum and 0.1% crystalline violet staining solution were purchased from Beijing Solarbio Science&Technology Co., LTD (China). Trypsin, Proteinase K, and Endopeptidase K were purchased from Sangon Biotech (Shanghai) Co., LTD (China). The BCA kit was purchased from Beijing Zoman Biotechnology Co., LTD (China). LPS from *E. coli* O111:B4 was purchased from Sigma-Aldrich (USA). The CCK-8 kit was purchased from the Dojindo Laboratories (Japan). The Mouse TNF-α ELISA Kit and Mouse IL-6 ELISA Kit were purchased from Elabscience Biotechnology Co. LTD (Wuhan, China). FAM-labeled single random sequence DNA with 22 bases (F-DNA) was synthesized and obtained from Takara Biotechnology Co., Ltd (Dalian, China). The standard strains used in this work were purchased from Shanghai Luwei Technology Co. LTD (China). All aqueous solutions used are prepared from ultrapure water. All reagents are used directly without any purification.

Fluorescence spectra were recorded on a Cary Eclipse fluorescence spectrophotometer (Agilent Technologies, USA). Ultraviolet–visible

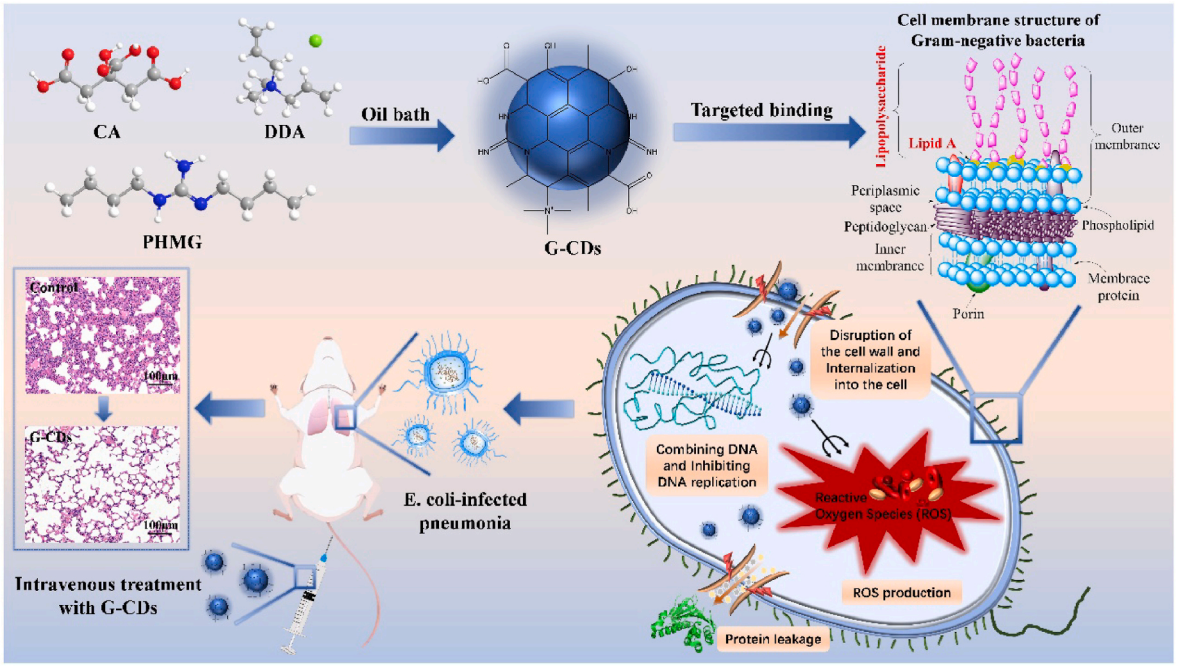

Scheme 1. Schematic illustration of the synthesis of G-CDs, the antibacterial mechanism and the *in vivo* treating of infected pneumonia.

(UV–vis) absorption spectra were measured on a UV-2450 UV–visible spectrophotometer (Shimadzu Corporation, Japan). Fourier Transform Infrared Spectroscopy (FTIR) was collected using a NICOLET iS50 Infrared Spectroscopy (Thermo Fisher Scientific, USA). Transmission electron microscopy (TEM) images were performed on a FEI Talos F200S (Thermo Fisher Scientific, USA). The absorbance was recorded on a Multiskan GO Microplate Reader (Thermo Fisher Scientific, USA). Confocal laser scanning images (CLSM) were acquired on Leica SP5 (Leica, Germany).

2.2. Preparation of G-CDs

In a round bottom flask, 0.2 g of CA was heated at 150 °C with stirring. After the CA was completely melted, 2 ml of DDA (60% aqueous solution) was added and the reaction was continued for another 150 min. After the addition of 1 ml 0.1 g/ml PHMG, the reaction was continued for 60 min at 170 °C. After the reaction solution in the flask was cooled, the product was dialyzed (500–1000 D) in 1000 ml deionised water. Change the deionised water every 2 h for 48 h. Finally, the liquid in the dialysis bag was freeze-dried to obtain solid G-CDs and stored at 4 °C for further study.

2.3. Bacterial culture and preparation of bacterial solutions

All the test bacteria were inoculated on agar plates by the plate scribing method and incubated at 37 °C to obtain single colonies, which were inoculated in sterilized saline (0.9% NaCl solution) to obtain a bacterial suspension. The turbidity of the bacterial suspension was measured and adjusted to 0.5 to obtain a bacterial suspension of 1.5×10^8 CFU/ml using a Mackenzie turbidimeter.

2.4. In vitro antibacterial experiments of G-CDs

Constant broth dilution experiment: Several sterile tubes were numbered sequentially and MH broth containing different concentrations of G-CDs was obtained by multiplicative dilution. One ml of the above MH broth and 1 ml of 1.5×10^6 CFU/ml bacterial suspension were added to each tube. A negative control (2 ml of blank broth) and a positive control (1 ml of blank broth plus 1 ml of 1.5×10^6 CFU/ml bacterial suspension) were set up. Finally, after incubation at 37 °C for 24 h, the lowest concentration tube with no bacterial growth was visually determined as the MIC of G-CDs on the test organisms.

Determination of the inhibition curve: the experiment was carried out as the constant broth dilution method to the incubation stage, 200 μl of suspension was taken in 96-well plates at 2 h intervals and OD_{600} values were measured immediately with a Microplate Reader, after 24 h, samples were taken and measured at 12 h intervals until the end of 48 h. The inhibition curve was plotted using the OD_{600} value as the vertical coordinate and time as the horizontal coordinate.

Evaluation of the stability of antibacterial properties: the MIC of the aqueous G-CDs solution was evaluated after storage at 4 °C for 1, 7, 14, 30, 60, 90, 120, 150, 180, 240 and 360 days according to a constant broth dilution assay. In addition, the aqueous solutions of G-CDs were subjected to continuous irradiation with a UV lamp (365 nm) for 2 h, water bath at 80 °C for 10 h, or incubation with the proteases of Trypsin, Proteinase K, and Endopeptidase K (final concentration of 10 mg/ml) at 37 °C for 8 h, respectively. And the MIC values of the above-treatment G-CDs were tested. The stability of G-CDs in serum was evaluated by measuring the antibacterial activity of G-CDs in MH broth containing 50% fetal bovine serum and 50% rabbit serum.

2.5. The anti-biofilm assay of G-CDs

Evaluation of the inhibition ability of G-CDs to the production of biofilm: 50 μl of 1.5×10^8 CFU/ml bacterial suspension and 50 μl of different concentrations of G-CDs solution were added to a 96-well plate. After incubation at 37 °C for 48 h, the plate with the discarded suspensions was washed three times with PBS. Then, each of the wells in the plate were fixed in methanol for 15 min, stained with 0.1% crystal violet for 15 min, and washed with PBS three times. Lastly, the stained layer was dissolved in 33% glacial acetic acid solution for the measurement of the OD_{570}.

Evaluation of the elimination effect of G-CDs on the mature biofilms: After the incubation of 100 μl of 1.5×10^8 CFU/ml bacterial suspension in a 96-well plate for 48 h, the suspensions were discarded and washed three times with PBS. Then, different concentrations of G-CDs were added for further incubation at 37 °C for 24 h. The residual biofilms were quantified by crystalline violet staining. Furthermore, the dyes of

SYTO 9/PI were applied to evaluate the elimination effect of G-CDs on the mature biofilms using CLSM. The experiment was repeated in a confocal dish for the later staining. The three types of bacteria were cultured in tryptic soy broth (TSB) medium at 37 °C for 72 h. The suspensions were discarded and washed three times with saline. Then, 320 μg/ml G-CDs were added for further incubation at 37 °C for 24 h. After washing with saline, the bacterial biofilms were stained with SYTO 9 and PI, and washed again with saline, then 3D and 2D images of bacterial biofilms before and after the action of G-CDs were observed by applying CLSM.

2.6. Live/dead bacteria staining test

One ml of 1.5×10^8 CFU/ml suspension was added to 1 ml of MH broth and incubated overnight at 37 °C, then 1 ml of G-CDs solution or saline was added and incubated for 4 h at 37 °C. The incubation solution was centrifuged at 3000 rpm for 15 min and washed three times with saline. After adding PI (final concentration of 10 μg/ml) for 15 min and DAPI (final concentration of 5 μg/ml) for 5 min, the bacteria were washed three times with saline and dispersed in saline. Then, the staining of bacteria with/without G-CDs was observed by CLSM.

2.7. Membrane depolarization assay

Bacterial cells were washed and resuspended to obtain an OD_{600} of 0.5 with saline. The 3,3-dipropylthiadicarbocyanine iodide (DiSC3(5)) of the final concentration of 0.5×10^{-6} M was added. After incubation at room temperature, the fluorescence intensity was measured with excitation wavelength at 622 nm and emission wavelength at 670 nm with an interval of 10 min for 30 min. After 30 min, G-CDs or saline was injected. The fluorescence intensity of bacterial suspensions in the presence G-CDs or saline was measured with an interval of 10 min for 30 min. Enhanced fluorescence intensity of bacterial suspensions is positively correlated with the dissipated membrane potential.

2.8. Extracellular protein concentration assay

The colonies were dispersed in MH broth and incubated overnight at 37 °C. After centrifugation at 3000 rpm for 15 min, the precipitate was washed three times with saline. Then the bacterial suspension was dispersed in saline to be with the control of $OD_{600} = 0.5$. One hundred μl of different concentrations of G-CDs were added to 900 μl of bacterial suspension and incubated at 37 °C for 4 h. After centrifugation at 8000 rpm for 5 min, the 100 μl of supernatant was collected and the extracellular protein concentration was quantified according to the procedure of the BCA kit.

2.9. Measurement of ROS in bacteria

One ml of G-CDs solution or saline was added to 1 ml of 1.5×10^8 CFU/ml bacterial suspension and incubated for 2 h at 37 °C. Then, the solution was centrifuged at 3000 rpm for 15 min and washed three times with saline for the further incubation of 2′,7′-dichlorodifluorofluorescein diacetate (DCFH-DA, final concentration of 10 μM) for 20 min at 37 °C. The ROS production of bacteria with/without G-CDs was monitored using a fluorescence spectrophotometer and CLSM.

2.10. Evaluation of the interaction of G-CDs with DNA

One hundred μl of different concentrations of G-CDs were added to 100 μl of PBS buffer containing F-DNA (final concentration of 50 nM), respectively. After incubation for 10 min at room temperature in dark, the fluorescence spectra of FAM were monitored for the evaluation of fluorescence quenching efficiency (F_0–F/F_0). F and F_0 are the fluorescence intensities of DNA at 520 nm in the presence or absence of G-CDs, respectively.

2.11. The influence of LPS and metal cations on the MIC of G-CDs

One ml of different concentrations of LPS or KCl, $MgCl_2$, $ZnCl_2$, and $CaCl_2$ solutions (final concentration of 50 μg/ml) were added to each grouped tube containing different concentrations of G-CDs, respectively. The MIC of incubated G-CDs against *E. coli* was tested according to the constant broth dilution method.

2.12. The absorption of LPS on G-CDs

One hundred μl of G-CDs solution (final concentration of 10 μg/ml) was added to 100 μl of PBS containing F-DNA (final concentration of 100 nM). After incubation at room temperature in dark for 10 min, the system of G-CDs and F-DNA was divided into two tubes. One hundred μl of this system was added to 100 μl of different concentrations of LPS, and another divided system was diluted using 100 μl PBS. The reaction was carried out for 10 min at room temperature in dark. The fluorescence emission spectra were measured exciting at 488 nm using a fluorescence spectrophotometer and the desorption rates were calculated.

2.13. Examination of the interaction of G-CDs with DNA

The quenching system solution was obtained according to the experimental method in 2.12. After the addition of 100 μl of PBS buffer into the 100 μl of the quenching system, the fluorescence of this reaction system was monitored continuously for 5 min. Correspondingly, another 100 μl of the quenching system was added with 100 μl denaturants of 3 M NaCl or 10 mM sodium pyrophosphate or 1 mM adenosine or 5 M urea or 0.01% SDS or 0.01% CTAB or 0.01% Triton X-100 or 0.01% Tween-80 or 50% DMSO for the immediate monitor of the fluorescence in the continuous 55 min. And the desorption rate (F/F_0) was calculated. F and F_0 are the fluorescence intensities of DNA at 520 nm in the presence or absence of denaturants, respectively.

2.14. Evaluation of resistance of bacteria to G-CDs

On the basis of the constant broth dilution experiment, the drug resistance assessment was performed according to previous work [43]. First, the initial MIC of G-CDs against *E. coli*, *S. aureus* and MRSA were obtained by the constant broth dilution experiment. Then, the suspension of the sub-MIC tubes was spread on an agar medium and incubated at 37 °C. The bacteria obtained from the incubation were prepared in saline in a new bacterial dilution (about 1.5×10^8 CFU/ml) and used in the next MIC detection. Repeated the steps and record the MIC until the MIC at day 30 was obtained and compared with the initial MIC to determine the development of drug resistance.

2.15. Effect of G-CDs on bacterial ATP levels

Bacterial cells were washed and resuspended to obtain an OD_{600} of 0.5 with saline. After treating by various concentrations of G-CDs for 4 h, bacterial cultures were centrifuged at 3000 rpm for 15 min, and the supernatant was applied for ATP levels testing using ATP assay kit.

2.16. Effect of G-CDs on bacterial efflux pumps

Bacterial cells were washed and resuspended to obtain an OD_{600} of 0.5 with MH broth. Ethidium bromide (EtBr) with the final concentration of 5 μM was added to the suspension, followed by Carbonyl cyanide 3-chlorophenylhydrazone (CCCP, 100 μM), G-CDs and MH broth, respectively. After incubation at 37 °C, the fluorescence intensity was measured with excitation wavelength at 300 nm and emission wavelength at 600 nm with an interval of 10 min for 60 min. And the fluorescence intensity change values ($\triangle F = F - F_0$) were calculated. F and F_0 are the fluorescence intensity of the suspension at the present and initial moments, respectively.

2.17. Hemolysis test of G-CDs

With the consent of the healthy volunteers, human blood samples were obtained from the 900th Hospital of Joint Logistics Support Forces of the Chinese PLA.

The blood was centrifuged at 1500 rpm for 15 min, the red blood cells were collected and dispersed in 1 ml of saline. After washing, 4% red blood cell dispersion in saline was prepared. Then, 750 μl of red blood cell dispersion was mixed with 750 μl of saline containing different concentrations of G-CDs. After incubation at 37 °C for 3 h, the supernatant from the centrifugation at 12000 rpm for 15 min was applied to determine the OD_{540} for the calculation of the hemolysis rate. The pure saline and water were applied as negative control group and positive control group according to the parallel operation, respectively.

2.18. In vitro cytotoxicity assay of G-CDs

Both BEAS-2b cells and Hacat cells were cultured in RPMI Medium 1640 medium containing 10% (v/v) fetal bovine serum and 1% (v/v) penicillin at 37 °C and 5% CO_2. After 24 h of incubation in 96-well plates, cells were added to culture medium containing different concentrations of G-CDs for the advanced incubation for 6, 12 or 24 h. The liquid in the plates was replaced with medium containing 10% CCK-8 and incubated for 2 h, and the OD_{450} values were measured for the calculation of the cell viability.

2.19. In vivo safety evaluation of G-CDs

The *in vivo* experiments were approved by the Experimental Animal Ethics Committee of Fujian Medical University and operated in accordance with the Guide to Animal Experiments (Ethical number: IACUC FJMU 2022–0009). All clean-grade ICR mice ("mice") were purchased from the Laboratory Animal Center of Fujian Medical University (Production License No.: SCXK (Fujian) 2016–0002).

Healthy mice were intravenously administrated with saline and G-CDs of different concentrations (50, 500, and 2000 μg/ml) once daily at a dose of 0.1 ml/10 g according to their body weight. After the continuous administration of 14 d, the rats from the different groups were applied to blood biochemical analysis (AST, ALT, CREA, BUN, and UA) and pathological analysis. Moreover, the other rats were also applied to the same blood and pathological evaluation after the 7-day rest after the 14-day continuous administration.

2.20. Evaluation of the in vivo antibacterial activity of G-CDs in a mouse pneumonia model of E. coli infection

To simulate HAP caused by G^- bacteria, a mouse pneumonia model of *E. coli* infection was developed. Twenty-four 20 ± 3 g mice were randomly divided into 4 groups. The healthy group was fed normally. One hundred-twenty μl of *E. coli* suspension (6×10^8 CFU/ml) was dropped into the nasal cavity of other rats in 6 doses. One day later, the experimental group (G-CDs) and positive control group (levofloxacin) were treated with G-CDs solution (500 μg/ml) and levofloxacin solution (50 μg/ml) by intravenous injections (IV) at a dose of 0.1 ml/10 g, respectively. The negative control group was given the same dose of saline. After one day of the intervention, the blood was obtained for blood routine analysis (WBC and NEUT). One hundred μl homogenate of the lung was spread on a plate and incubated at 37 °C for 24 h to calculate the residual bacteria in the lung. And the TNF-α and IL-6 levels of the homogenate were detected through ELISA. Additionally, the pathological evaluation of rat's lung from different groups was carried out using hematoxylin and eosin (H&E) staining and immunohistochemical analysis.

2.21. Statistical analysis

All experiments in this work were repeated three times, and the data were expressed as mean ± standard deviation (SD). Statistical comparisons were analyzed by One-way ANOVA Tukey's multiple comparisons tests using Graph Pad Prism 8 [(ns) not significant, $P > 0.05$, $^*P < 0.05$, $^{**}P < 0.01$, $^{***}P < 0.001$, and$^{****}P < 0.0001$].

3. Results

3.1. Characterization of G-CDs

A simple two-step thermal decomposition method was developed to prepare G-CDs (Fig. 1A). The water contact angle of G-CDs was measured to be 28.94 ± 0.5° (Fig. 1B), indicating the hydrophilicity of G-CDs. The morphology of G-CDs studied in TEM (Fig. 1C) shows that the G-CDs are quasi-spherical particles with good dispersion and homogeneity. The average size of G-CDs is 2.38 nm. High-resolution TEM suggests that the lattice spacing of G-CDs is 0.24 nm, which is consistent with the interlayer spacing of graphitic carbon [44]. The optical properties of G-CDs were investigated. As shown in Fig. 1D, the UV–vis absorption spectrum of G-CDs illustrates an absorption peak and a shoulder peak at 230 nm and 310 nm, respectively, which are attributed to the π→π* and n→π* transitions of G-CDs [45]. The G-CDs dispersion appears as a yellow transparent liquid in the visible light and blue illustration excited by UV. The G-CDs exhibit a fluorescence emission spectrum with a maximum emission of 393 nm at an optimal excitation of 310 nm. Fig. 1E shows that G-CDs have an excitation-dependent property in the excitation range from 280 to 370 nm. And the emission peaks gradually red-shift with gradually increased excitation wavelengths.

The functional groups of G-CDs were analyzed. As shown in the FTIR spectra (Fig. 1F), the absorption peaks of DDA at 3023 cm^{-1} and 2977 cm^{-1} are attributed to the asymmetric stretching vibration (V^{as}) and symmetric stretching vibration (V^{s}) of the C–H, respectively [46]. Using DDA as the feedstock, the asymmetric stretching vibrations (V^{as}) and symmetric stretching vibrations (V^{s}) of the C–H at 3019 cm^{-1} and 2972 cm^{-1} are found in the FTIR of G-CDs, indicating the presence of alkane chains. The absorption peaks of DDA and G-CDs at 1476 cm^{-1} are attributed to the bending vibration (δ) in the shear plane of the C–H attached to $–N^+(CH_3)_3$ [47], indicating the presence of quaternary ammonium. The absorption peaks of PHMG at 1620 cm^{-1} and G-CDs at 1632 cm^{-1} are both attributed to the bending vibration (δ) of the N–H of the guanidinium group [48]. Moreover, the absorption peaks of PHMG at 1356 cm^{-1} and G-CDs at 1365 cm^{-1} are attributed to C–N single bond stretching vibrations (V) in the guanidine group [49]. The kept peaks of the guanidinium group in G-CDs confirm the successful guanidinylation of G-CDs. In addition, the absorption peaks of G-CDs at 959 cm^{-1} and 881 cm^{-1} may be generated by the stretching vibrations (V) of the bonds of C–C and C–O, respectively.

Meanwhile, XPS was applied to evaluate the elemental composition and functional groups of G-CDs. Full-wavelength XPS mapping of G-CDs (Fig. 1G) shows the three main typical peaks attributed to C1s (284.91 eV), N1s (401.86 eV), and O1s (531.57 eV) with the atomic contents of 80.32%, 9.88%, and 9.8%, respectively. The four fitting bands of the high-resolution C1s spectra (Fig. 1H) are attributed to C–C (284.6 eV), C–N (285.7 eV), C–O (286.3 eV), and C═N (287.8 eV), respectively [50]. Three binding energies of the high-resolution N1s spectra (Fig. 1I) can be found at 399.4 eV, 401.7 eV, and 402.2 eV, which are assigned to $C{=}NH_2^+$, $(C–NH_2^+)$ and positively charged quaternary ammonium $(-N^+(CH_3)_3)$ [51,52]. In addition, the high-resolution peak of O–C (Fig. 1J) at 531.57 eV is obtained at the fitted spectrum of O1s [53]. The chemical structure of G-CDs was further characterized using NMR. The peak signals between 20 and 100 ppm in the ^{13}C NMR spectrum (Fig. 1K) are ascribed to C–C, C–N, and C–O sp^3 hybridized aliphatic C atoms. While the peaks between 100 and 140 ppm are assigned to C═N sp^2 hybridized C atoms [54]. ^1H NMR spectrum (Fig. 1L) shows that G-CDs

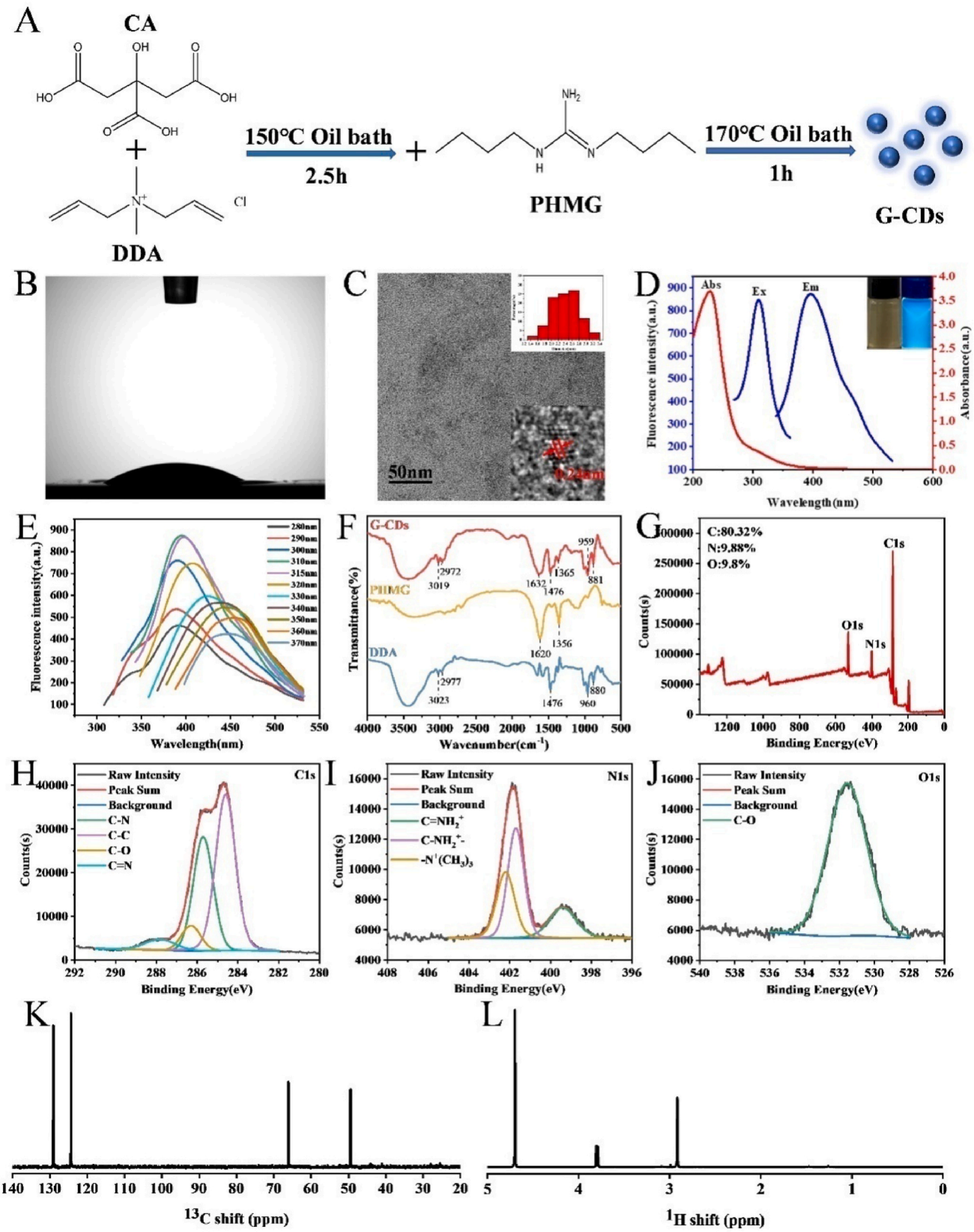

Fig. 1. Preparation scheme and Characterization of G-CDs. (A) The two-step melting process. (B) Water contact angle measurement diagram. (C) TEM image with size distribution (upper) and HRTEM (bottom). (D) UV–Vis and fluorescence spectra. (E) Fluorescence spectra at different excitation wavelengths. (F) FTIR spectra. (G–J) XPS spectra and high-resolution XPS spectra of C1s, N1s, and O1s. (K, L) ^{13}C NMR spectrum (101 MHz, D_2O) and ^{1}H NMR spectrum (400 MHz, D_2O). (A colour version of this figure can be viewed online.)

exhibit peaks corresponding to aliphatic hydrogens at 1–2 ppm, and those at 2–4 ppm could be attributed to specific functional groups of CH–N and N–H. The large resonance at 4.69 ppm is corresponding to the O–H group, which may be from D_2O. The NMR spectra prove that G-CDs have a hybrid structure including sp^2 and sp^3 carbon atoms. Overall, the results of FTIR, XPS, and NMR infer that the N doping effect, the bonds of C–C, C–O, and C═O, quaternary ammonium group, and guanidine are mainly present in G-CDs.

3.2. In vitro antibacterial properties of G-CDs

The effects of G-CDs on *E. coli* (ATCC25922), *S. marcescens* (CMCC(B) 41002), *Salmonella paratyphi B* (CMCC(B)50094), *S. aureus* (ATCC6538), MRSA (ATCC43300), *E. faecalis* (ATCC29212), *S. epidermidis* (ATCC12228) and *L. monocytogenes* (ATCC19115) were evaluated through the constant broth dilution test. As shown in Table S1, the MIC values of G-CDs to the eight common bacteria suggest the strong and broad-spectrum antibacterial activity of G-CDs. The MIC of G-CDs for *S. epidermidis* and *L. monocytogenes* are 2.5 μg/ml, and for *S. aureus* and MRSA are both 5 μg/ml. And G-CDs have a MIC of 10 μg/ml against *E. coli* and *S. marcescent*. G-CDs demonstrate slightly stronger inhibition against G^+ bacteria than G^- bacteria, and also retain the same strong antibacterial activity against drug-resistant strains. The MIC values of G-CDs on nine resistant strains of bacteria isolated from the clinic were also measured by the constant broth dilution test. As shown in Table S2, using the inhibition ability of G-CDs against the standard strains as a comparison, the MIC values of G-CDs against the above nine clinically resistant bacteria are the same as those of the corresponding positive and negative bacteria, indicating that G-CDs still have superior antimicrobial activity against clinically resistant bacteria, and predicting the feasibility of the application of G-CDs in clinical infections caused by drug-resistant bacteria.

Using *E. coli*, *S. aureus,* and MRSA as model bacteria, the OD_{600} values of broth after the action of different concentrations of G-CDs on bacteria at different periods were measured. As shown in Fig. S2, the OD_{600} values of the three bacterial broths in the blank group (Control) were small at the initial 4 h, indicating the weak growth of the three bacteria at the inception phase. Then, the exponentially increased OD_{600}

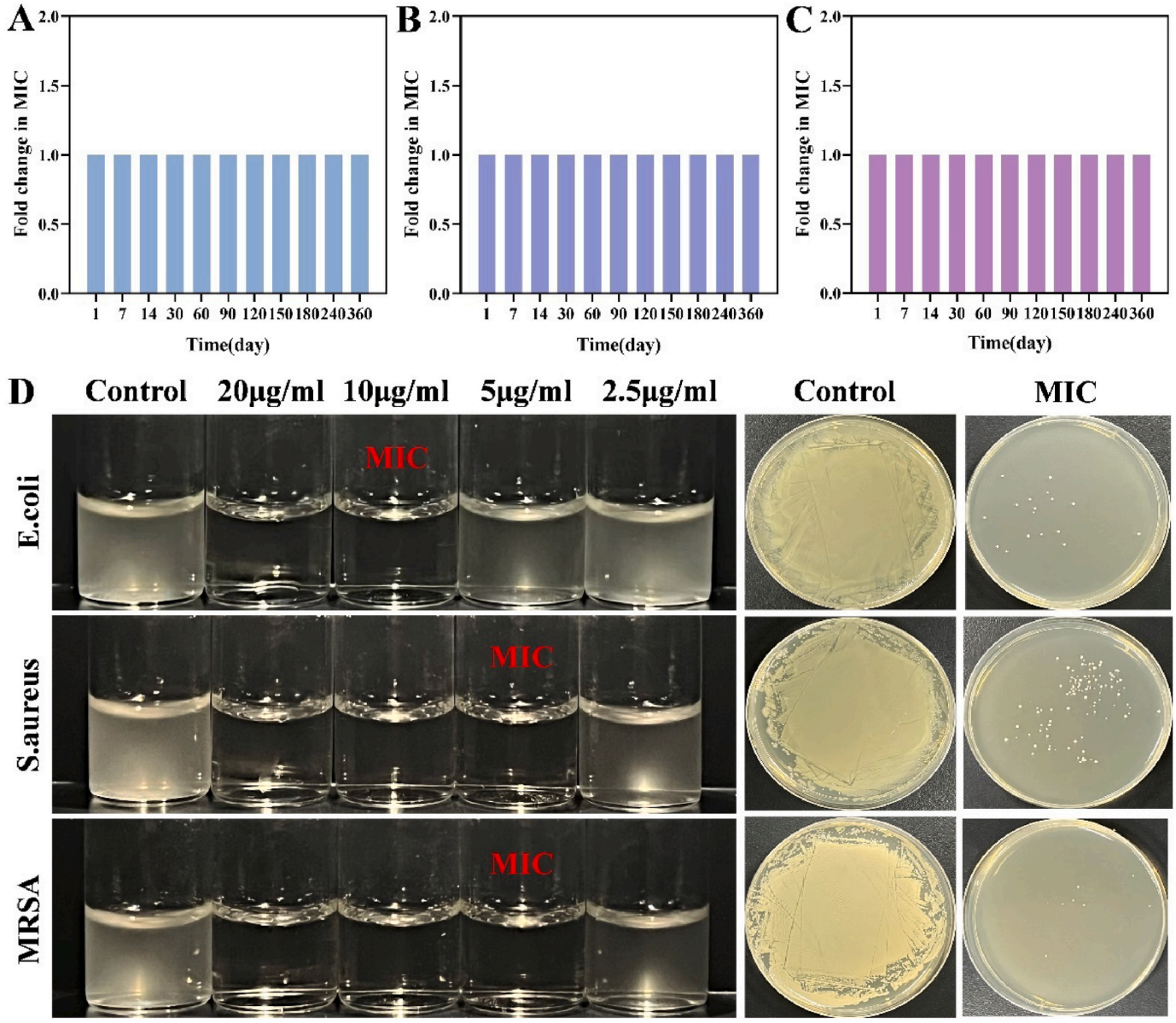

Fig. 2. Long-term stability of antimicrobial properties of G-CDs. (A) Against *E. coli.* (B) Against *S. aureus.* (C) Against MRSA. (D) Experimental phenomena and colony diagrams of G-CDs in constant broth dilution experiments after 360 days of storage at 4 °C. (n = 3).

values implied that the bacteria were proliferating rapidly after more than 4 h. According to the MIC values of G-CDs, different concentrations of G-CDs were set to investigate the inhibitory effects of G-CDs on different bacteria. When the concentration of G-CDs is lower than MIC, the time points at which the OD_{600} values of the three bacteria appeared to increase within 24 h are delayed with the increase of G-CDs (Fig. S2). Although it shows a similar regular with the blank group after 24 h, the OD_{600} values decrease with the increase of G-CDs, indicating that G-CDs with sub-MIC concentrations could play a certain degree of inhibition against the selected bacteria. In contrast, G-CDs at the MIC show strong inhibition on the three bacteria within 48 h, indicating that G-CDs have good broad-spectrum antibacterial activity and show concentration-dependent behavior.

Besides the evaluation of MIC, the long-term antimicrobial stability of G-CDs is a significant and prerequisite performance index for possible clinical applications based on the real preservation requirement. Although the long-term antimicrobial performance of antimicrobial nanomaterials was evaluated in some studies (e.g. Table S3), the long-term stability of the antimicrobial properties of many reported antimicrobial carbon dots or nanomaterials are unclear. The maintenance of the antimicrobial activity of G-CDs after prolonged storage was investigated against *E. coli*, *S. aureus*, and MRSA, as shown in Fig. 2. In the 360 days of storage, the MIC values of G-CDs remain unchanged since the initial period, indicating the excellent long-term stability of antibacterial performance. In addition, considering the complexity of the external environment as well as the *in vivo* condition, the stability of the antimicrobial properties of G-CDs in different ambient conditions was assessed. As shown in Fig. S3, G-CDs exhibit stable antibacterial activity under continuous UV irradiation (365 nm) and high temperature. Moreover, the antimicrobial activity of G-CDs is almost kept under the interference of 50% fetal bovine serum (FBS) or 50% rabbit serum, and even after co-incubation with trypsin, protease K and recombinant protease K, respectively. The stable antimicrobial property of G-CDs in long-term storage and possible interfering conditions illustrates the expected and acceptable antimicrobial agent for real applications.

3.3. *In vitro anti-biofilm property of G-CDs*

It has been reported that 80% of bacteria can develop to produce biofilms by adhering to certain carrier surfaces to form microflora containing colonized bacteria [55]. The production of biofilms is one of the terrible triggers for the development of bacterial resistance, and bacteria that form biofilms are 10–1000 times more resistant to antibacterial drugs than planktonic bacteria [56,57]. The inhibition ability of G-CDs on the biofilm formation and the eradication property of G-CDs on the formed biofilm were systematically evaluated. After co-incubation of different concentrations of G-CDs with *E. coli*, *S. aureus,* and MRSA for 48 h, the production rates of bacterial biofilm were compared with the group without G-CDs, as shown in Fig. 3A–C. Increased contents of G-CDs induce decreased biofilm production. When incubated with 20 μg/ml G-CDs, the rate of *E. coli* biofilm decreases to about 43%, and the rate of *S. aureus* and MRSA biofilm are almost zero. When the concentration of G-CDs reaches 40 μg/ml, the production of *E. coli* biofilm is almost completely inhibited, indicating the excellent inhibition ability of G-CDs to the production of biofilm (Fig. 3A–C). The performance of G-CDs in eliminating bacterial mature biofilms was evaluated. As shown in Fig. 3D–F, all of the formed biofilms are gradually disrupted with increasing concentrations of G-CDs. When the concentration of G-CDs is 40 μg/ml, up to 93% of *E. coli* mature biofilms are eradicated. And the 40 μg/ml G-CDs can destruct about 60% of both *S. aureus* and MRSA biofilms. Moreover, less than 23% of both *S. aureus* and MRSA biofilms are residual with the introduction of 320 μg/ml G-CDs. In addition, the disrupting ability of G-CDs to mature biofilms was investigated using SYTO 9 and PI. SYTO 9 can permeate the cell

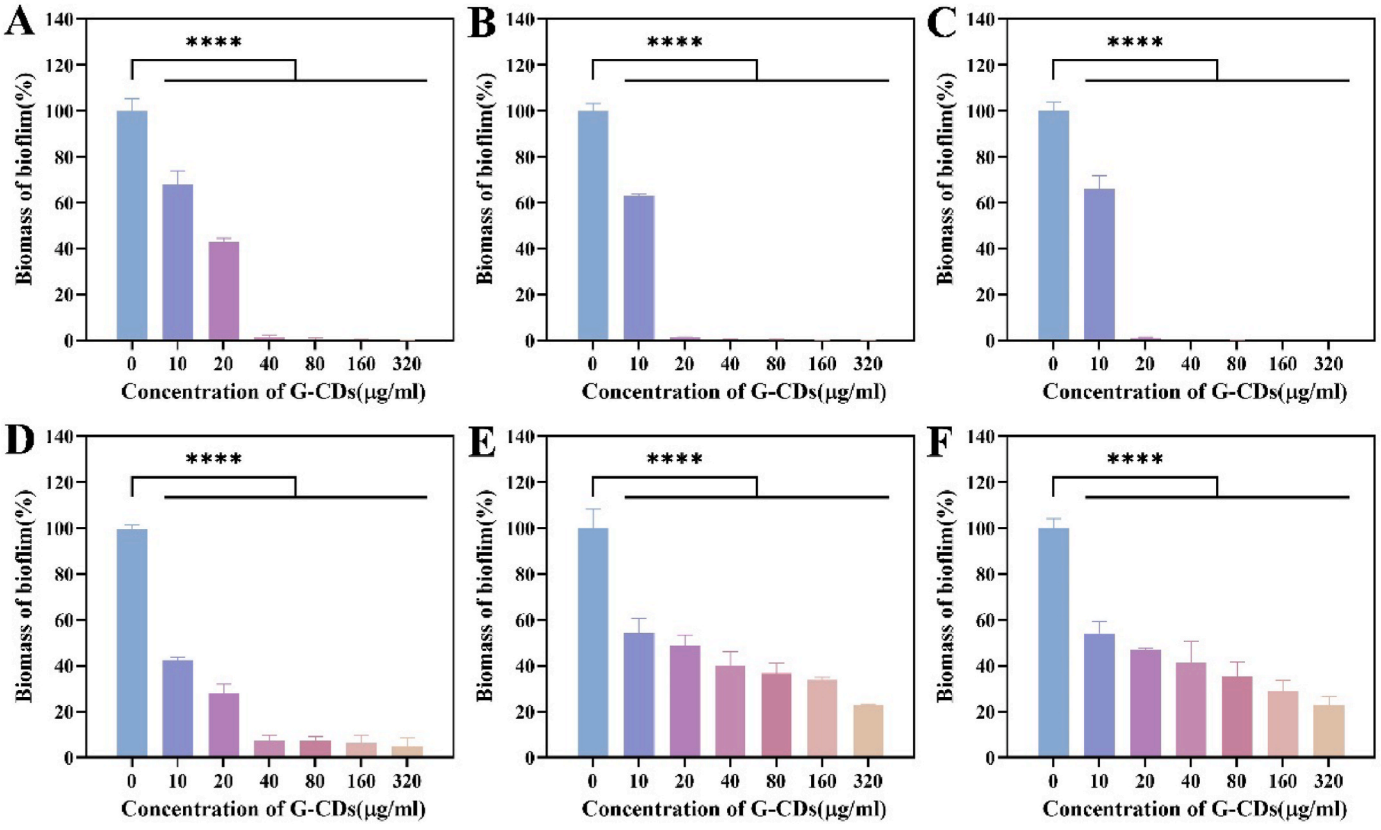

Fig. 3. Anti-biofilm properties of G-CDs. (A–C) Performance of G-CDs in inhibiting biofilm production by *E. coli*, *S. aureus,* and MRSA. (D–F) Performance of G-CDs in eliminating mature biofilms of *E. coli*, *S. aureus,* and MRSA. [n = 3, ****$P < 0.0001$]. (A colour version of this figure can be viewed online.)

membranes and label all bacteria with green fluorescence, while PI can specifically stain dead bacterial cells with red emitting. As shown in Fig. S4, untreated bacterial biofilms exhibit bright green fluorescence signals but little red emission. The integrity of bacterial biofilms with G-CDs were destroyed with the distinctive red fluorescent signals (Fig. S4). The thickness of the biofilms was significantly reduced, indicating the death of a large number of bacteria and the destruction of mature biofilms. G-CDs possess small nano size, positive charges conferred by quaternary ammonium and guanidine groups, and hydrophilicity, enabling them to interact and fuse with biofilms. These properties facilitate the entry of G-CDs into the basal layer of biofilms and contribute to the disruption of bacterial biofilms [58–61]. The phenomenon observed by CLSM is consistent with the results of crystalline violet staining, which further demonstrate that G-CDs have antibacterial efficacy against planktonic bacteria and colonized bacteria.

3.4. Antibacterial mechanism of G-CDs

E. coli, *S. aureus,* and MRSA were used as representatives of G^-, G^+, and drug-resistant bacteria to study the antibacterial mechanisms of G-CDs, respectively. First, the state of the live/dead bacteria before and after the action of G-CDs was evaluated by the staining of DAPI/PI, as shown in Fig. 4A. Little red fluorescence but full of blue staining is observed in the untreated bacteria. However, after the action of G-CDs, the bacteria show intense red fluorescence but a weakened blue illustration, indicating G-CDs alter bacterial cell membrane permeability and lead to massive bacterial death, which implies the effective killing effect of G-CDs on bacteria. Furthermore, the action of G-CDs on the bacterial structure was initially investigated by SEM, as shown in Fig. 4A. The untreated bacteria show an intact and smooth cell membrane. The cell wall and cell membrane of the bacteria were significantly wrinkled or even ruptured after the interaction with G-CDs, and even the cell contents were disintegrated and leaked. The effect of G-CDs on bacterial membrane potential was further assessed using DiSC3(5) as a membrane potential sensitive probe that aggregates within the phospholipid bilayer. When the membrane is depolarized, the membrane potential is lost with the increased fluorescence in solution from the released DiSC3 (5). As shown in Fig. 4B–D, DiSC3(5) interacts with bacteria and accumulates in the bacterial cell membrane with a weak fluorescence in solution. At the 30th min, the addition of G-CDs/saline (Control) showed no significant change in the fluorescence of the control group. However, the addition of G-CDs causes an obvious increase in the fluorescence intensity of all three bacterial fluids and further increased with the duration of action, indicating the loss of bacterial membrane potential, suggesting that bacteria undergo depolarization after G-CDs treatment. The extracellular protein concentrations of the three bacteria after interaction with different concentrations of G-CDs were determined using a protein quantification method (Fig. 4E–G). The extracellular protein concentrations of all three bacteria gradually increase with the increase of G-CDs, showing a certain concentration dependence, which is in accord with the inhibition exhibition of G-CDs (Fig. S2). These results indicate that G-CDs can cause damaging effects containing depolarization of bacterial cell membranes to bacteria, and then lead to the leakage of cytoplasmic components and the disruption of bacterial cell walls and cell membrane integrity.

The action of the antimicrobial agent with the bacterium is the key to its antimicrobial activity [62]. Correspondingly, the possible production of intracellular ROS was initially evaluated using DCFH-DA as a probe. As shown in Fig. S5, DCFH-DA shows weak fluorescence centered at 525 nm after interacting with G-CDs, *E. coli*, *S. aureus,* and MRSA alone. When G-CDs interacted with bacteria, the incubated DCFH-DA produces obvious fluorescence at 525 nm, indicating that the absorption of G-CDs in bacteria could produce ROS. The fluorescence intensities detected in *S. aureus* and MRSA after interaction with the same concentration of G-CDs are higher than that in *E. coli*, indicating that the same content of G-CDs causes more ROS in *S. aureus* and MRSA than that in *E. coli*. The different degrees of inspired ROS may be one of the key reasons for the different antibacterial activities of G-CDs against various types of bacteria. Meanwhile, CLSM images (Fig. S6) visualize the production of green fluorescence of 2′,7′-Dichlorofluorescein (DCF) caused by the formation of intracellular ROS before and after the action of G-CDs using DCFH-DA as a probe [43]. It shows that G-CDs can penetrate and promote ROS production in the bacterial cells to play a killing effect on the bacterium. Furthermore, considering the potential destructiveness of generated ROS to common cells, the possible amount of ROS generated by G-CDs and cells was investigated. Using Hacat cells as a representative, the same dose of G-CDs induces almost little green fluorescence in the cells (Fig. S7), indicating that G-CDs do not cause excessive ROS in the cells. This result implies that G-CDs may interact differently with bacteria and cells, which is a significant factor for the development of an antimicrobial agent with strong antimicrobial activity and acceptable biocompatibility.

Besides the production of ROS after the entering of G-CDs, the potential interaction between G-CDs and DNA was also evaluated. Using F-DNA as the model gene, the interaction between G-CDs and the intracellular gene was carried out. As shown in Fig. S8A, F-DNA possesses a high fluorescence intensity at 520 nm, however, the fluorescence of F-DNA is gradually quenched with the addition of increased G-CDs. Fig. S8B shows that the quenching degree of F-DNA can reach about 90% after the addition of G-CDs at a concentration of 2 times the MIC, indicating that G-CDs can effectively adsorb and interact with DNA. The absorption and interaction of G-CDs to DNA will drastically induce the conformation and even function of DNA [43,63]. In summary, the antibacterial mechanism of G-CDs is mainly through the interaction and penetration of G-CDs on bacterial cell walls and cell membranes, and the further entry of G-CDs produces excessive ROS in bacteria and the interfering of the gene. Such multiple interactions inhibit and even combat the growth and reproduction of bacteria to the ultimate death of bacteria.

G-CDs can effectively interact and combat G^- bacteria, which is significantly enhanced compared with the reported antibacterial carbon dots [33,34,64,65]. While the cell wall structure of G^- bacteria is very different from that of G^+ bacteria, the antibacterial mechanism, especially for the absorption and interaction of G-CDs against G^- bacteria may be different from that of G^+ bacteria. It has been validated that enhancing the interaction between agents and bacteria and then being swallowed by bacteria is an important way to improve the antibacterial properties of agents [66]. The elucidation of the enhanced antibacterial property of G-CDs against G^- bacteria was further carried out based on the reinforced interaction of G-CDs and the membrane structure of G^- bacteria. Compared with the reported mainly electrostatic and hydrophobic actions of antibacterial carbon dots on G^+ bacteria, the interacting modes of absorption between G-CDs and the cell wall of G^- bacteria were investigated.

First, the changed surface charge of the interaction of G-CDs and bacteria was monitored. As shown in Fig. 5A, the Zeta potential of G-CDs was tested to be +5.6 mV, indicating the positively charged surface. The Zeta potentials of *E. coli*, *S. aureus*, and MRSA confirm the negative charge of the bacterial cell membrane. While the Zeta potentials of all three bacteria were positively shifted after interacting with G-CDs, indicating that G-CDs can interact with the bacterial surface through electrostatic interaction. However, the degree of the positive shift of the Zeta potential of the interacting system of *E. coli* and G-CDs is significantly lower than that of *S. aureus* and MRSA, suggesting that the strength of the electrostatic interaction between G-CDs and *E. coli* is weaker than that of *S. aureus* and MRSA. This is consistent with several reported antibacterial nanomaterials about the acting mode mainly through electrostatic interaction for the fact that the antibacterial activity is better on G^+ bacteria than that on G^- bacteria [67,68].

Based on the fluorescent performance of G-CDs, the CLSM was further applied to compare the adsorption performance of G-CDs on

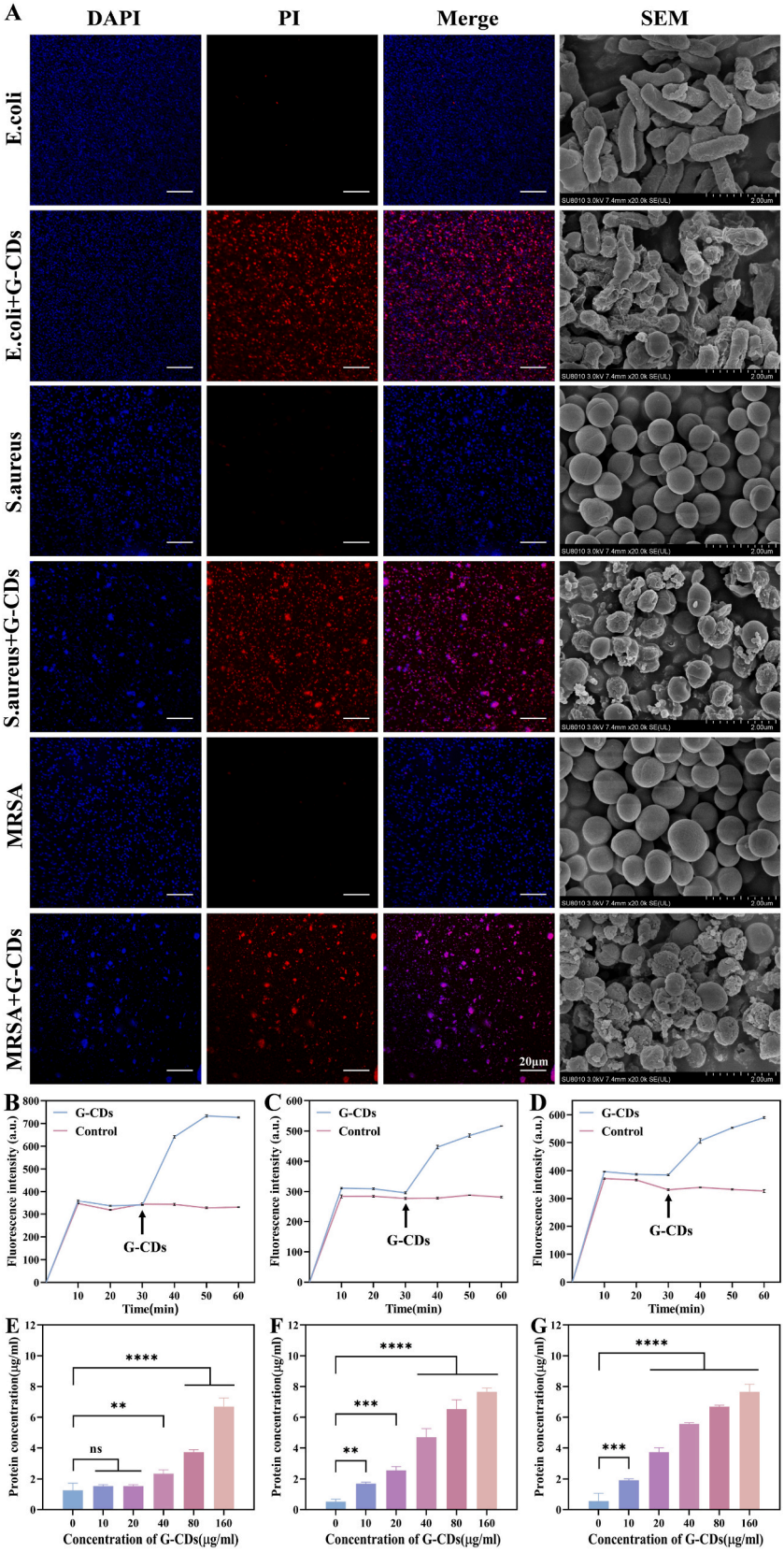

Fig. 4. Interaction of G-CDs with cell membranes of *E. coli*, *S. aureus* and MRSA. (A) CLSM images of Live/Dead-stained bacteria and SEM images. (B–D) The monitoring of the Bacterial cell membrane potential levels using DiSC3(5) as probe. (E–G) Bacterial extracellular protein levels. [n = 3, (ns) not significant, $P > 0.05$, $^{**}P < 0.01$, $^{***}P < 0.001$ and $^{****}P < 0.0001$]. (A colour version of this figure can be viewed online.)

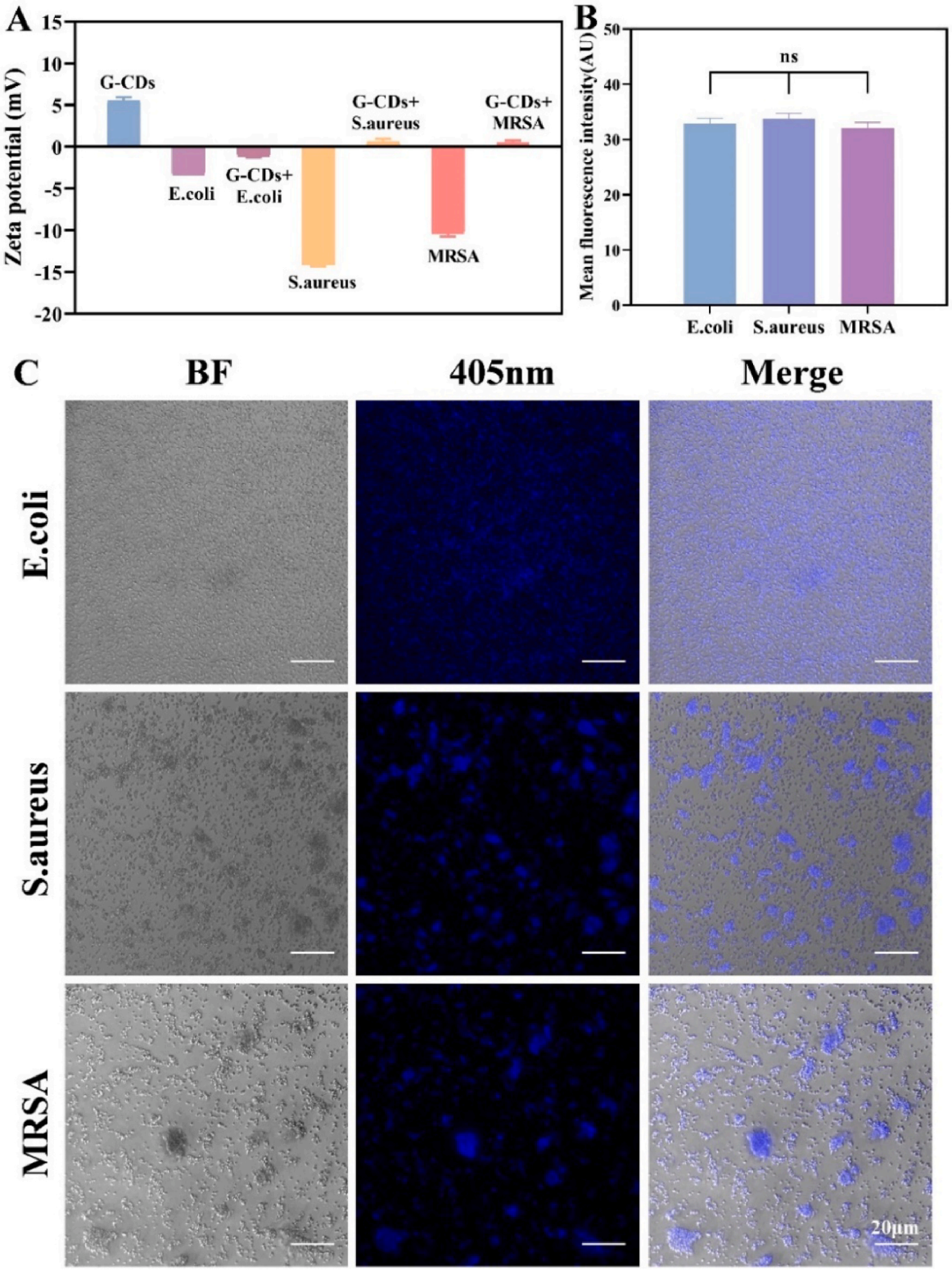

Fig. 5. Interaction of G-CDs with bacterial surfaces of *E. coli, S. aureus* and MRSA. (A) Zeta potential. (B) Quantification of fluorescence intensity of CLSM images. (C) CLSM images. [n = 3, (ns) not significant, $P > 0.05$].

different bacterial surfaces. As shown in Fig. 5C, *E. coli*, *S. aureus,* and MRSA show bright blue fluorescent illustrations with the introduction of G-CDs, suggesting the absorption and staining of G-CDs on bacteria. Meanwhile, the average fluorescence intensities of G-CDs adsorbed on the three bacteria at the same concentration are very similar according to the fluorescence quantification results (Fig. 5B), indicating that the adsorption capacity of G-CDs on the three bacteria is close. The close absorption activity of G-CDs against G^- bacteria and G^+ bacteria will promote G-CDs to effectively engage with G^- bacteria like that of G^+ bacteria. Compared with the stronger electrostatic interaction of G-CDs and G^+ bacteria, there should be some other interaction forces in addition to electrostatic interaction between G-CDs and G^- bacteria.

The key difference in the outer membrane between G^- bacteria and G^+ bacteria is that the G^- bacteria have a protective membrane layer mainly composed of LPS. *E. coli*-derived LPS was applied as a model to assess the role of G-CDs against the outer membrane of G^- bacteria. As shown in Fig. 6A, the antibacterial activity of G-CDs against *E. coli* shows a concentration-dependent inhibition by the added LPS, indicating that the exogenously added LPS could compete with bacteria to bind G-CDs [69]. The competition of LPS suggests that LPS reduces the binding of G-CDs to the bacterial surface and thus weakens antibacterial activity, which confirms the binding effect of G-CDs on G^- bacteria through the LPS. Since the main component of lipid A in LPS can be neutralized by divalent cation bridges through electrostatic interactions [70], the effect of metal cations on the antibacterial activity of G-CDs was further exploited to examine whether G-CDs can bind to the section of lipid A in LPS. As shown in Fig. 6B, the presence of Ca^{2+} causes significant inhibition of the antibacterial activity. This result reveals that G-CDs might compete with Ca^{2+} for binding to lipid A, suggesting that G-CDs can effectively bind to lipid A in the outer membrane LPS of G^- bacteria besides electrostatic interaction, thereby enhancing surface interactions with G^- bacteria. In addition, based on the ability of G-CDs to both bind LPS and F-DNA, the quenching system of the absorbed F-DNA on G-CDs was introduced to test whether the addition of LPS completes and desorbs F-DNA from G-CDs [71,72]. As shown in Fig. 6C and D, the fluorescence of F-DNA gradually recovers with increased LPS, indicating that the interaction of LPS on G-CDs is stronger to replace the absorbed DNA [71,72]. The results have led to a deeper reflection and provided a new way of thinking to further explore the interaction forces between G-CDs and LPS. The interaction modes of G-CDs and LPS will infer the possible interaction forces between G-CDs and the surface of G^- bacteria. As the confirmed model of nanomaterials and ssDNA for the acting forces of nanomaterials to biomolecular, the absorption system of G-CDs and ssDNA was introduced for the studying of the interaction forces between G-CDs and LPS [73–77]. The denaturants were introduced into the absorption and quenching system of the complex of G-CDs and F-DNA to displace DNA from G-CDs by monitoring the restored fluorescence for the characterization of the interaction mode [73,76,78]. Each denaturant indicates correspondingly different types of intermolecular force [73,76,78]. NaCl, sodium pyrophosphate, adenosine, urea, and DMSO indicate the electrostatic attraction, phosphate backbone adsorption, nuclei base adsorption, hydrogen bonding, and hydrophobic interactions, respectively [79–81]. Meanwhile, SDS, CTAB, Triton X-100, and Tween-80 as surfactants of different molecular weights are indicated as the presence or absence of vdW forces. As shown in Fig. S9, the introduction of 3 M NaCl causes over 80% of the DNA to detach from the G-CDs, indicating an electrostatic attraction between the G-CDs and the negatively charged DNA. However, A total of 0.01% SDS causes almost 100% fluorescence recovery of F-DNA from G-CDs. There are two possible reasons for the stronger desorption of DNA by G-CDs due to the

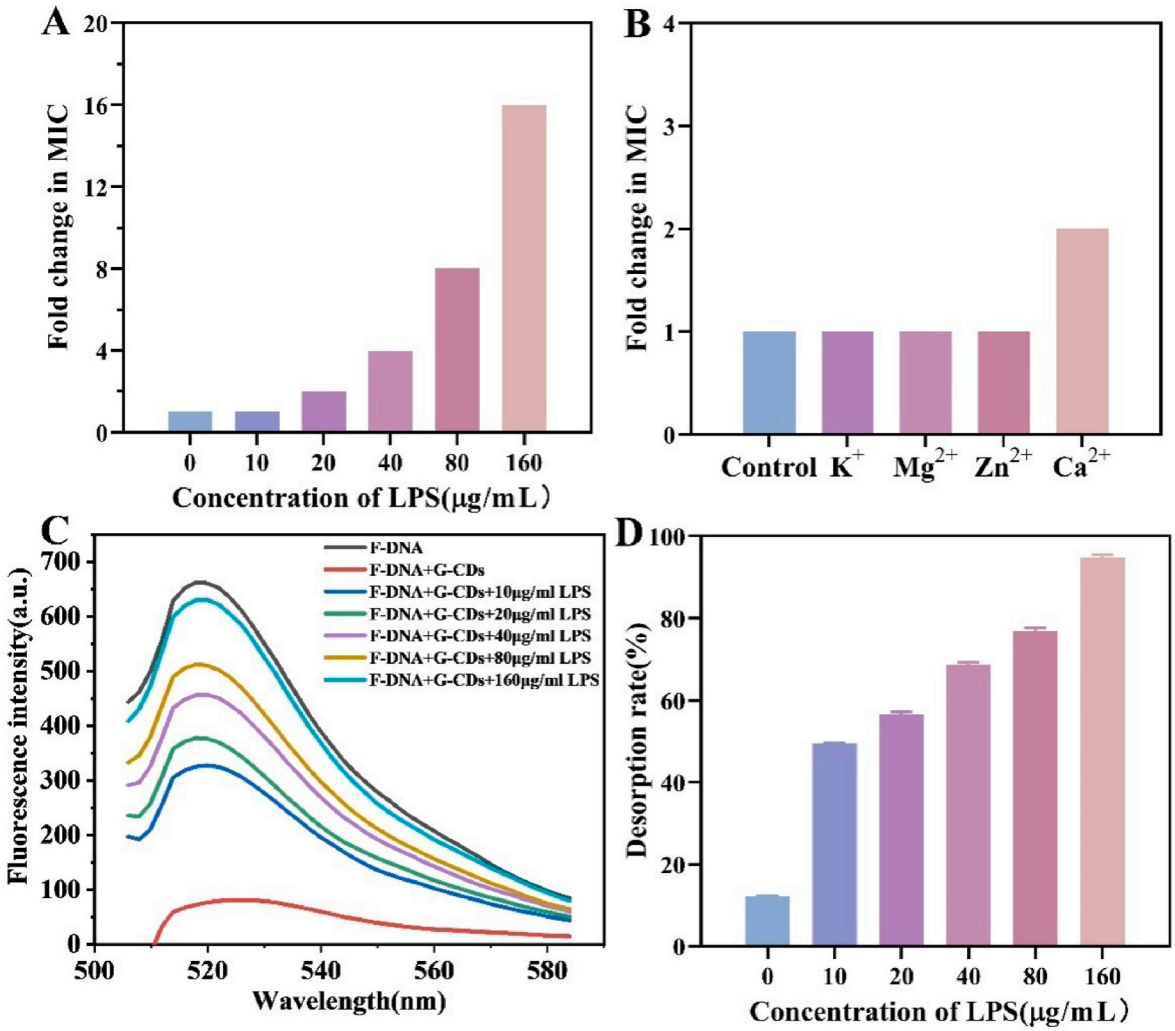

Fig. 6. Interaction of G-CDs with LPS. (A) Antibacterial activity of G-CDs against *E. coli* in the presence of different concentrations of LPS. (B) Antibacterial activity of G-CDs against *E. coli* in the presence of different metal ions. (C) Fluorescence spectra of G-CDs and F-DNA quenching system in the presence of different concentrations of LPS. (D) Desorption rates of G-CDs and F-DNA quenching system in the presence of different concentrations of LPS. (n = 3).

addition of SDS. As a kind of anionic surfactant, SDS has a hydrophobic tail that can desorb DNA through vdW force actions with G-CDs. Moreover, the presence of ionic SDS increases the salt concentration to weaken the electrostatic attraction between DNA and G-CDs for DNA desorption. In addition, 5 M urea, 0.01% CTAB, and 10 mM sodium pyrophosphate have evident but weak desorption effects on G-CDs. Summarizing the results in the graph it can be seen that the strength of the interaction between G-CDs and DNA specifically includes: vdW force > electrostatic adsorption > hydrogen bonding > phosphate backbone adsorption > hydrophobic interaction ≈ nucleobase adsorption, indicating that G-CDs mainly adsorb DNA by vdW force, electrostatic adsorption, and hydrogen bonding. Analogically, we conjecture that G-CDs may also act on the surface of G^- bacteria by vdW force, electrostatic adsorption, and hydrogen bonding on the LPS. Such multimode interactions of G-CDs and LPS, the main outer membrane component of G^- bacteria, may promote the absorption of G-CDs on G^- bacteria to enhance the antibacterial activity.

3.5. Evaluation of inducing bacterial resistance to G-CDs

Acquired bacterial resistance is a significant concern for the design of drugs for real application. The resistance profile of bacteria chronically exposed to G-CDs was assessed. *E. coli*, *S. aureus* and MRSA were incubated with G-CDs for 30 consecutive days at sub-MIC concentrations. As shown in Fig. 7A–C, the MIC values of G-CDs against the above three bacteria remain unchanged during 30 days of continuous incubation, indicating that G-CDs possess antimicrobial activity without detectable resistance. Meanwhile, the strain identification (Fig. S10) shows that no mutation of bacteria was found after 30 days of continuous incubation, suggesting that G-CDs may be an effective antimicrobial material with

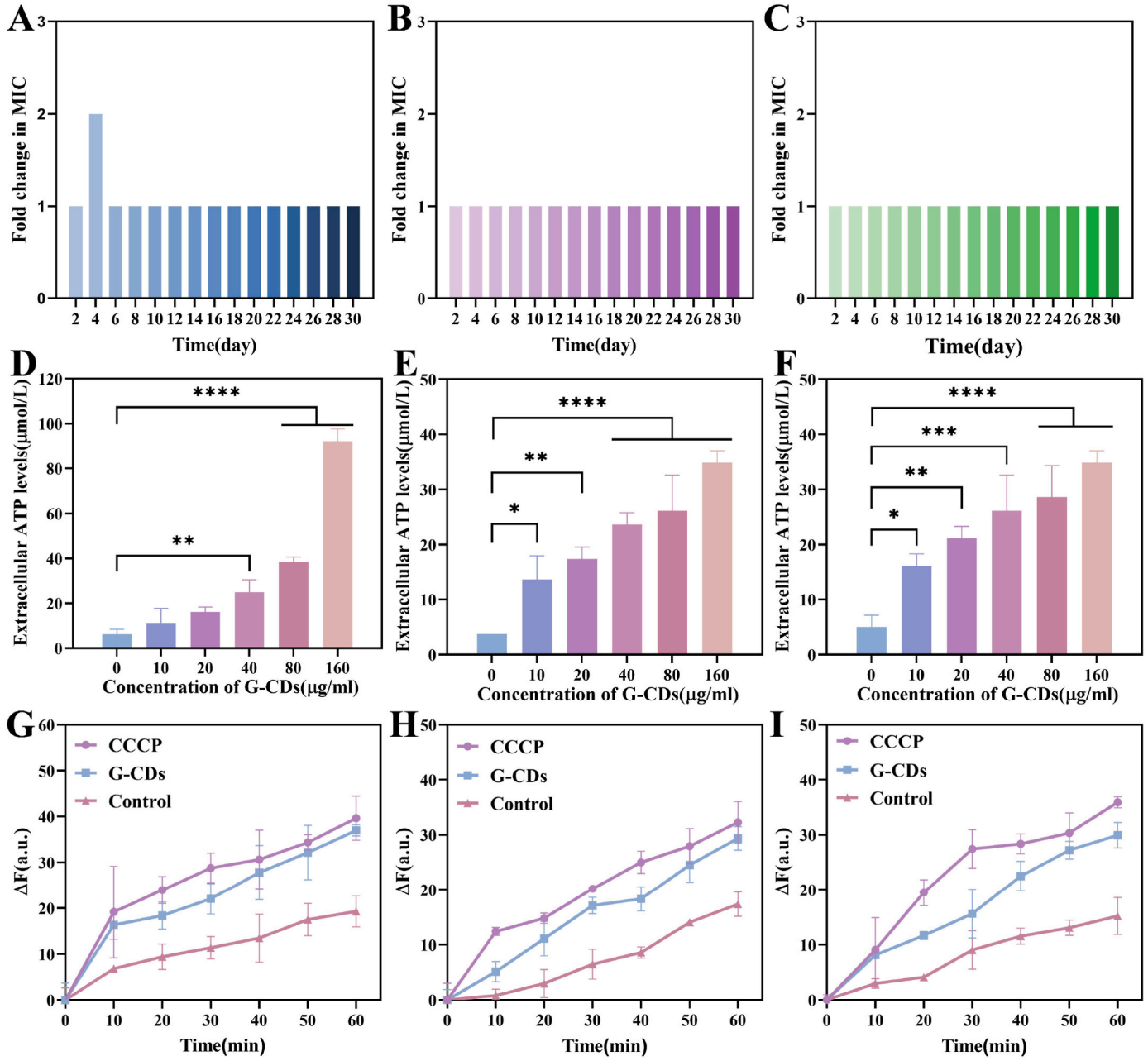

Fig. 7. Bacterial resistance to G-CDs and its mechanism. (A–C) Resistance profiles of *E. coli*, *S. aureus* and MRSA. (D–F) Effect of G-CDs on the extracellular ATP level of *E. coli*, *S. aureus* and MRSA. (G–I) Effect of G-CDs on the efflux pump activity of *E. coli*, *S. aureus* and MRSA through fluorescence using EtBr as probe. [n = 3, $^*P < 0.05$, $^{**}P < 0.01$, $^{***}P < 0.001$, and $^{****}P < 0.0001$]. (A colour version of this figure can be viewed online.)

the avoidance of the worry about drug induced resistance.

To elucidate the mechanism by which G-CDs do not induce drug resistance in bacteria, we evaluated the effect of G-CDs on bacterial ATP levels and bacterial efflux pump activity. As shown in Fig. 7D–F, under the action of different concentrations of G-CDs, the extracellular ATP levels of the three bacteria increase in a concentration-dependent manner, indicating that the presence of G-CDs significantly increase the efflux of ATP within the bacteria. The survival, growth and reproduction of bacteria need to convert nutrients into energy through metabolism and eliminating metabolic waste. Compared with eukaryotic cell, bacteria mainly rely on ATP for energy metabolism related reactions due to the lack of mitochondria. This increased release of ATP with introduced G-CDs indicates that G-CDs can inhibit the growth and reproduction of bacteria by reducing their ATP levels, ultimately exhibiting antibacterial and bactericidal effects. ATP is essential for the bacterial efflux pump to function [82]. The bacterial efflux system is the main resistance mechanism of the bacteria [83]. When bacteria are exposed to antibiotics for a long time, it may cause overexpression of bacterial efflux pumps, thereby promoting the excretion of antibiotics, reducing drug concentration in the bacterial body, and leading to antibiotic resistance. EtBr, as a toxic dye, enters the bacterial body and induces active efflux. Therefore, by comparing the accumulation of EtBr in the bacterial body, the activity of the bacterial efflux pump can be determined. EtBr was applied as the fluorescent probe to evaluate the activity of bacterial efflux pumps before and after exposure to G-CDs, as shown in Fig. 7G–I. In the normal bacterial group (Control), due to the normal expression of bacterial efflux pumps, EtBr accelerates efflux, and the accumulation of EtBr in the bacterial body is relatively small. Therefore, there is little change in fluorescence intensity. Correspondingly, the addition of efflux pump inhibitor (CCCP) significantly inhibits the expression of bacterial efflux pumps, and EtBr accumulates extensively in the bacterial body, resulting in a significant increase in fluorescence intensity. However, after adding G-CDs of MIC value (Fig. 7G–I), the fluorescence intensities are significantly higher than that of the normal bacterial group and show a similar trend as the CCCP group. This indicates that the presence of G-CDs significantly increases the accumulation of EtBr in the bacterial body, suggesting that G-CDs have a certain degree of inhibitory effect on bacterial efflux pump activity. The inhibitory effect on bacterial efflux pump activity may be a key factor that G-CDs do not induce bacterial resistance.

3.6. Safety evaluation of G-CDs

In vitro hemolysis assay was carried out to evaluate the effect of G-CDs on erythrocytes. As shown in Fig. S11A, when red blood cells were added to sterilized water, they rupture due to the difference of osmotic pressure inside and outside the cells, and the solution is red after centrifugation. In contrast, when incubated with different concentrations of G-CDs in saline, erythrocytes were deposited at the bottom after centrifugation with the colorless and transparent supernatant. When the concentration of G-CDs reached 12 times of the MIC, the hemolysis rate was still less than 5% compared with the negative control (Fig. S11B), indicating that G-CDs do not cause erythrocyte rupture and have good hemocompatibility under physiological conditions.

The *in vitro* cytotoxicity of G-CDs and raw material of PHMG on BEAS-2b cells and Hacat cells at different times were investigated using a CCK-8 kit. As shown in Figs. S11C–F, G-CDs do not have a significant effect on the survival of either cell types under the same conditions of 4-fold MIC value and 24 h of action, with a survival rate of about 80%. However, only low contents of PHMG caused both cells to almost completely die. Furthermore, G-CDs at a concentration of 6-fold MIC value maintained more than 80% survival of both BEAS-2b cells and Hacat cells within 6–12 h, while the survival rates of the incubation with PHMG are poor. The results indicate that PHMG is more cytotoxic to BEAS-2b and Hacat cells than the G-CDs synthesized from PHMG. However, G-CDs at a concentration of 8-fold MIC value show reduced survival of both cells after 24 h of incubation, which may be due to the poor selectivity of G-CDs with broad-spectrum antimicrobial activity [30]. It is necessary to point out that higher concentrations (about 8-fold MIC) of G-CDs can exert some cytotoxic effects on eukaryotic cells as the increased acting period. In the clinic, the blood concentration of antibiotics from MIC to C_{max} (maximum blood concentration) are sufficient to achieve the effective bactericidal or bacteriostatic level [84]. Thus, combined with the strong combating effect of G-CDs against clinically resistant strains at MIC value and the *in vitro* cell safety of G-CDs at 4-fold MIC, it is implied that the G-CDs will meet the practical requirements. In addition, it has been reported that the biotoxicity of some antibiotics (e.g. aminoglycoside antibiotics) does not directly correlate with the blood drug concentration [84]. It is also unknown whether the biotoxicity of carbon dots correlates directly with blood concentration. Further studies are needed to assess the biotoxicity of carbon dots.

Further investigation of the *in vivo* biosafety of G-CDs is critical to the clinical applications of G-CDs. For the *in vivo* evaluation of the biosafety of G-CDs, the entire *in vivo* experiment was carried out based on the maximum of the simulation of clinical drug administration, treatment, and evaluation [85–87]. Tail vein administration was introduced to examine the effects of three dose levels of G-CDs at low, medium, and high (equivalent to a blood concentration in circulating blood volume of MIC, 10-fold MIC, 40-fold MIC) on body weight, blood biochemistry, and five major organs of the heart, liver, spleen, lung and kidney. During the 14-day treatment period, all mice showed normal activity, diet and mental status, and no abnormal signs such as reduced diet and depression were observed. As shown in Fig. 8A, the body weight of the mice in each group shows a similar pattern of change. Fig. 8B–F show that the levels of various blood biochemical indexes were very similar between the mice in different doses of G-CDs and saline groups without significant difference, suggesting that the liver and kidney functions of mice in different groups were well. The pathological sections stained by H&E (Fig. 8G) show that the tissue structure of the organs in the different groups with variable doses of G-CDs were not significantly different from that in the saline group, implying that G-CDs do not produce pathological damage to the five major organs of mice. Meanwhile, in order to investigate the cumulative chronic toxicity of G-CDs, a batch of mice was administered in the same manner for 14 days and then kept for following 7 days without administration. And then, the levels of five blood biochemical parameters and the pathological analysis of the five major organs were assessed and compared. As shown in Fig. S12, the different groups of mice still maintained almost the same results as the saline group, showing no *in vivo* toxicity or pathological damage of G-CDs. The results show that even high doses (40-fold MIC) of G-CDs exhibit almost no *in vivo* biotoxic effects, implying the feasibility of clinical applications.

3.7. Application of G-CDs in a mouse pneumonia model of E. coli infection

HAP is a threatening disease to people, and more than 60% of HAP are caused by G^- bacteria [88,89]. A mouse pneumonia model infected by *E. coli* was applied to evaluate the *in vivo* activity of G-CDs. Each group of mice had intervened through tail vein injection based on the clinical concerns about the route of administration. As shown in Fig. 9A–C, the lungs of mice in the saline group (negative control group) are infected with a large number of *E. coli*, and the levels of WBC, NEUT, TNF-α, and IL-6 are significantly elevated compared to the healthy group, indicating the successful model of HAP. After the intervention, the number of bacteria in the lungs of mice in the levofloxacin group (positive control group) and the G-CDs group (experimental group) are significantly reduced with a similar amount of bacteria colonies. Meanwhile, the levels of WBC, NEUT, TNF-α, and IL-6 in both treated groups are significantly reduced compared to the negative control group, and the values are almost the same as those in the healthy group without statistical difference. In addition, H&E-stained sections of lung

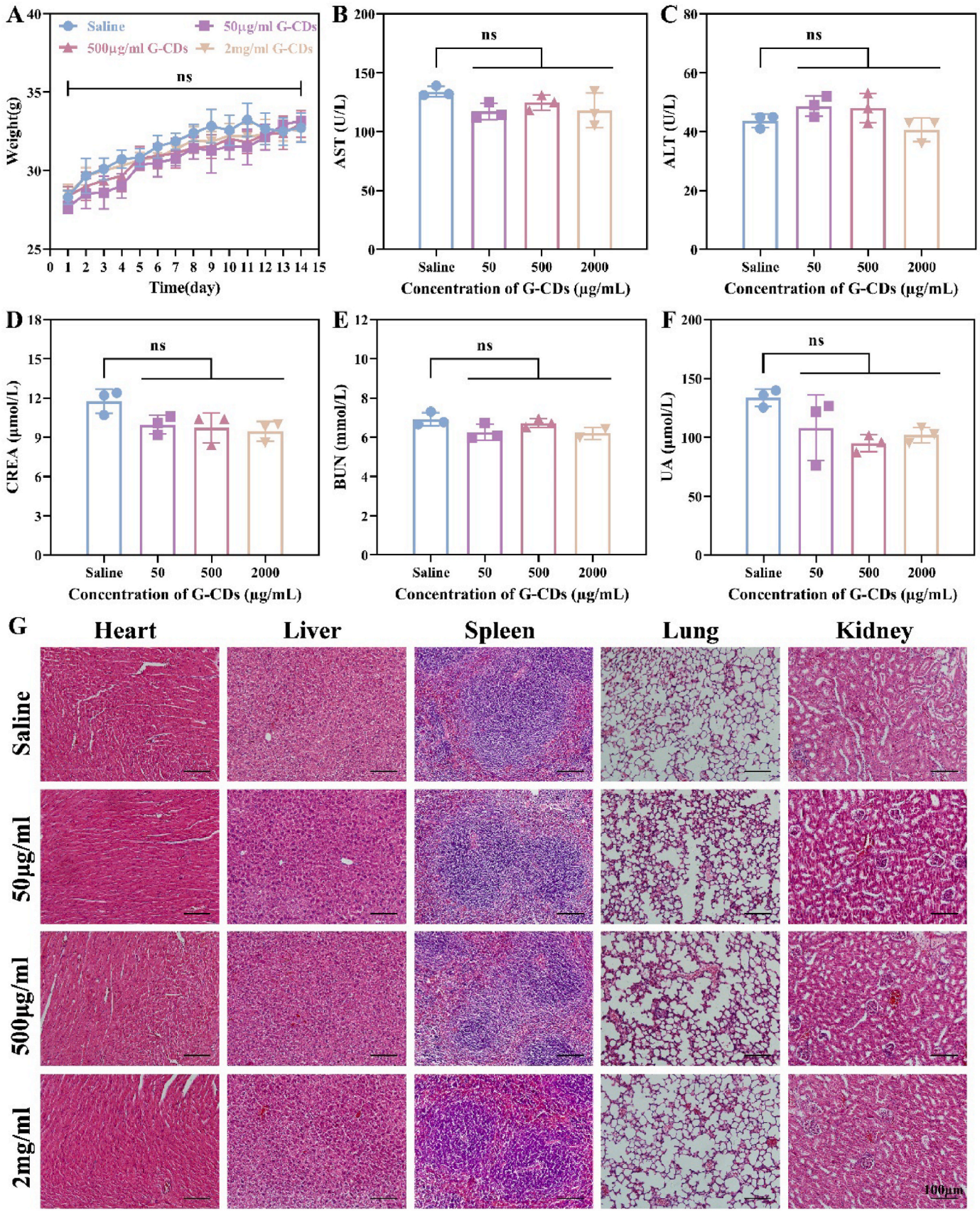

Fig. 8. Effect of continuous intravenous administration of G-CDs for 14 days on mice. (A) Body weight. (B, C) Blood biochemical liver function levels. (D–F) Blood biochemical kidney function levels. (G) H&E-stained sections of major organ tissues. [n = 3, (ns) not significant, $P > 0.05$].

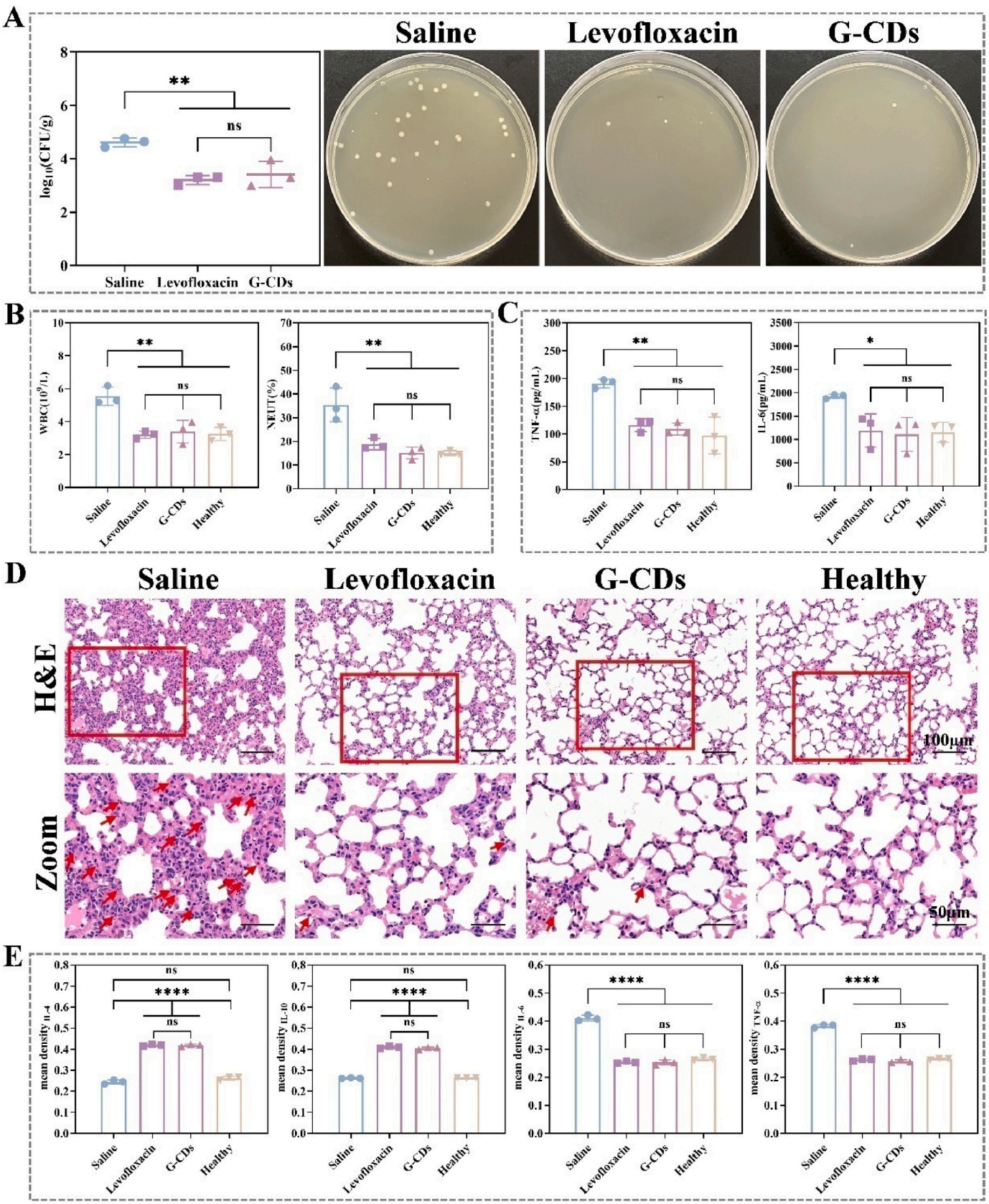

Fig. 9. The antibacterial capacity of G-CDs in a mouse pneumonia model of *E. coli* infection. (A) The number of bacteria in the lungs. (B) Levels of inflammatory indexes (WBC and NUET) in blood. (C) Levels of inflammatory factors (TNF-a and IL-6) in lungs. (D) H&E-stained sections of lung tissue. (E) Quantification of inflammatory factor levels in immunohistochemically stained sections of lung tissue. [n = 3, (ns) not significant, $P > 0.05$, *$P < 0.05$, **$P < 0.01$, ****$P < 0.0001$.].

tissue (Fig. 9D) show a significant increase in the distribution of neutrophils in the negative control group, along with pathological changes associated with the inflammatory responses of alveolar fusion, septal expansion, and congestion. In contrast, the levofloxacin and G-CDs groups show a significantly lower number of neutrophils, a normal alveolar structure, approaching the overall morphological structure of the healthy group, and a significant improvement in pathological changes such as congestion. Immunohistochemical evaluations were operated to visualize the changes in the expression of inflammatory factors in the lung tissue of mice before and after the intervention (Fig. S13). The two anti-inflammatory factors (IL-4, IL-10) and the two pro-inflammatory factors (IL-6, TNF-α) were introduced for further quantification using Image J based on the stained sections. As shown in Fig. 9E, the expression levels of the two anti-inflammatory factors (IL-4 and IL-10) are lower in the saline and healthy groups but significantly increased in the levofloxacin and G-CDs groups. The increased IL-4 and IL-10 levels suggest the recovery effects of the treated groups. In contrast, the positive expression levels of the two pro-inflammatory factors (IL-6 and TNF-α) are significantly lower in the levofloxacin, G-CDs, and healthy groups compared to the saline group. The above results indicate that G-CDs possess strong *in vivo* antibacterial properties and therapeutic effects on *E. coli*-infected HAP like that of the dose of levofloxacin. Furthermore, the dose of G-CDs through the injection can promote the regression and improvement of inflammation in mice with pneumonia. The *in vivo* effect of G-CDs reflects the appreciably practical applications in future clinical treatments.

4. Discussion

In recent years, the emergence and spread of antibiotic resistance, specifically drug-resistant bacteria, have become a global public health problem [2]. G^- bacteria, in particular, have become a very problematic issue in clinical infections due to their tendency to develop drug-resistant bacteria and even biofilms [8]. Although new drugs for G^+ bacteria have made great progress and are gradually being developed for clinical trials, developing new drugs for G^- bacteria remains a challenge due to the unique structure of G^- bacteria. Small molecule drugs or antibiotics struggle to penetrate through the G^- bacteria and are susceptible to drug resistance [7]. Nanomedicine, specifically carbon nanomaterials, have excellent performance in antibacterial applications, and their therapeutic efficacy against bacterial infections has increasingly received considerable attention [17–19]. It has been reported that a variety of antimicrobial carbon dots with different properties have been developed for antimicrobial therapy, revealing the great prospect of carbon dots for antimicrobial applications [27–30]. However, so far, carbon dots remain less effective against G^- bacteria and little attention has been paid to their ability to resist bacterial biofilms [33,34]. Simultaneously, current researches have neglected the evaluation of the long-term stability of antibacterial activity of carbon dots and the systematic study of how to enhance the interaction with G^- bacteria.

In this study, we successfully synthesize broad-spectrum and potent G-CDs based on PHMG and other materials, with MIC as low as 10 μg/ml for several common G^- bacteria (Tables S1 and S2). Besides the good long-term stability (Fig. 2), G-CDs are effective against bacterial biofilms (Fig. 3, S4). Additionally, the enhancement of the performance of G-CDs to G^- bacteria was evaluated through the acting modes of G-CDs to G^- bacteria using the confirmed interacting mode of carrier materials and ssDNA [71–73]. Besides the electrostatic adsorption, G-CDs also play binding effect on LPS through the modes of vdW force and hydrogen bonding (Fig. S9). The multimode of interaction of G-CDs and G^- bacteria will promote the adsorption and entering of G-CDs to bacteria for the further inspiration of ROS and intracellular gene interference (Figs. S5–S8). Such approach is promised to develop new ways of fighting G^- and drug-resistant bacteria and to address the lack of relevant systematic studies. Moreover, G-CDs can also inhibit the development of drug resistance in bacteria by suppressing the overexpression of bacterial efflux pumps (Fig. 7). The *in vivo* safety of the antimicrobial carbon dots, like G-CDs in this work, was evaluated based on the clinical concerns. G-CDs have few *in vivo* adverse effects in organisms using multi-method and multi-indicator approaches (Fig. 8 and S12). G-CDs show good therapeutic effects on *E. coli*-infected pneumonia *in vivo*, through the elimination of bacteria in the lungs and the successfully down-regulating inflammatory factor levels (Fig. 9 and S13). The antibacterial effect of G-CDs on *in vivo* pneumonia with the following immunoregulation is significant in promoting rapid recovery from the infectious condition. However, more researches are still needed to further elucidate the specific processes by which carbon dots enter the bacteria, the detailed ways in which carbon dots cause multiple changes in the bacterium, and the reasons for not inducing the development of drug resistance.

5. Conclusion

In summary, a convenient and efficient method was developed for the preparation of G-CDs with excellent antibacterial ability. G-CDs exhibit enhanced activity to G^- bacteria and long-term stability for antibacterial applications. The mechanism of the enhanced absorption action of G-CDs to G^- bacteria is clarified. The *in vivo* investigations suggest the satisfactory biosafety of rats and the excellent treating effect of *E. coli*-infected pneumonia. The combination of stable and potent antibacterial activity with biocompatibility, inhibition of resistance development, and excellent *in vitro* and *in vivo* antibacterial performance suggests that G-CDs are promising new antibacterial agents for the treatment of clinically relevant pathogenic bacteria. At the same time, research related to the antibacterial mechanism also provides a promising basis for breaking the bottleneck in the development of anti-Gram-negative drugs.

CRediT authorship contribution statement

Xintian Zhang: Methodology, Data curation, Formal analysis, Visualization, Writing – original draft, Writing – review & editing. **XinXin Bai:** Methodology, Data curation, Formal analysis, Visualization, Writing – original draft, Writing – review & editing. **Xiaoqin Deng:** Methodology, Data curation, Visualization. **Kai Peng:** Data curation, Formal analysis. **Zongfu Zheng:** Data curation, Formal analysis. **Jiecheng Xiao:** Resources, Data curation. **Rui Zhang:** Resources, Data curation. **Zhengjun Huang:** Resources, Data curation. **Jianyong Huang:** Project administration, Formal analysis, Visualization. **Min Chen:** Project administration, Formal analysis, Visualization. **Shaohuang Weng:** Conceptualization, Formal analysis, Supervision, Project administration, Writing – original draft, Writing – review & editing.

Declaration of competing interest

The authors declare that they have no known competing financial interests or personal relationships that could have appeared to influence the work reported in this paper.

Acknowledgments

The authors thank the Public Technology Service Center Fujian Medical University and its staff member Mr. Zhihong Huang for their technical guidance and assistance on CLSM imaging in this work. The authors gratefully acknowledge financial support from the Joint Funds for the Innovation of Science and Technology, Fujian Province (Nos. 2021Y9081, 2021Y9007), the National Science Foundation of Fujian Province (Nos. 2020J011022, 2020J01626, 2022J01493), and the Fujian Provincial Health Technology Project (No. 2021GGA011, 2021CXA014).

Appendix A. Supplementary data

Supplementary data to this article can be found online at https://doi.org/10.1016/j.carbon.2023.118229.

References

[1] R. Laxminarayan, The overlooked pandemic of antimicrobial resistance, Lancet 399 (10325) (2022) 606–607.
[2] T. Krell, M.A. Matilla, Antimicrobial resistance: progress and challenges in antibiotic discovery and anti-infective therapy, Microb. Biotechnol. 15 (2022) 70–78.
[3] A. Govindaraj Vaithinathan, A. Vanitha, WHO global priority pathogens list on antibiotic resistance: an urgent need for action to integrate One Health data, Perspect. Public Health 138 (2018) 87–88.
[4] R. Huwaitat, A.P. McCloskey, B.F. Gilmore, G. Laverty, Potential strategies for the eradication of multidrug-resistant Gram-negative bacterial infections, Future Microbiol. 11 (2016) 955–972.
[5] Y. Qiao, Y. Xu, X. Liu, Y. Zheng, B. Li, Y. Han, Z. Li, K.W.K. Yeung, Y. Liang, S. Zhu, Z. Cui, S. Wu, Microwave assisted antibacterial action of Garcinia nanoparticles on Gram-negative bacteria, Nat. Commun. 13 (2022) 2461.
[6] Y. Ding, Z. Sun, R. Shi, H. Cui, Y. Liu, H. Mao, B. Wang, D. Zhu, F. Yan, Integrated endotoxin adsorption and antibacterial properties of cationic polyurethane foams for wound healing, ACS Appl. Mater. Interfaces 11 (2019) 2860–2869.
[7] Z. Breijyeh, B. Jubeh, R. Karaman, Resistance of gram-negative bacteria to current antibacterial agents and approaches to resolve it, Molecules 25 (6) (2020) 1340.
[8] D. Reynolds, J.P. Burnham, C. Vazquez Guillamet, M. McCabe, V. Yuenger, K. Betthauser, S.T. Micek, M.H. Kollef, The threat of multidrug-resistant/extensively drug-resistant Gram-negative respiratory infections: another pandemic, Eur. Respir. Rev. 31 (166) (2022), 220068.
[9] Y. Meguro, J. Ito, K. Nakagawa, S. Kuwahara, Total synthesis of the broad-spectrum antibiotic amycolamicin, J. Am. Chem. Soc. 144 (12) (2022) 5253–5257.
[10] O. Goethe, M. DiBello, S.B. Herzon, Total synthesis of structurally diverse pleuromutilin antibiotics, Nat. Chem. 14 (11) (2022) 1270–1277.
[11] X. Chen, J. Han, X. Cai, S. Wang, Antimicrobial peptides: sustainable application informed by evolutionary constraints, Biotechnol. Adv. 60 (2022), 108012.
[12] T. Nakaya, M. Yabe, E.H. Mashalidis, T. Sato, K. Yamamoto, Y. Hikiji, A. Katsuyama, M. Shinohara, Y. Minato, S. Takahashi, M. Horiuchi, S.I. Yokota, S. Y. Lee, S. Ichikawa, Synthesis of macrocyclic nucleoside antibacterials and their interactions with MraY, Nat. Commun. 13 (1) (2022) 7575.
[13] W.X. Liang, Q. Yu, Z.X. Zheng, J.Y. Liu, Q.N. Cai, S.P. Liu, S.M. Lin, Design and synthesis of phenyl sulfide-based cationic amphiphiles as membrane-targeting antimicrobial agents against gram-positive pathogens, J. Med. Chem. 65 (20) (2022) 14221–14236.
[14] S. Zeng, Z.K. Wang, C. Chen, X.S. Liu, Y. Wang, Q.X. Chen, J.Y. Wang, H.D. Li, X. J. Peng, J.Y. Yoon, Construction of rhodamine-based AIE photosensitizer hydrogel with clinical potential for selective ablation of drug-resistant gram-positive bacteria in vivo, Adv. Healthc. Mater. 11 (17) (2022), 2200837.
[15] J.R. Schultz, S.K. Costa, G.R. Jachak, P. Hegde, M. Zimmerman, Y. Pan, M. Josten, C. Ejeh, T. Hammerstad, H.G. Sahl, P.M. Pereira, M.G. Pinho, V. Dartois, A. Cheung, C.C. Aldrich, Identification of 5-(Aryl/Heteroaryl)amino-4-quinolones as potent membrane-disrupting agents to combat antibiotic-resistant gram-positive bacteria, J. Med. Chem. 65 (20) (2022) 13910–13934.
[16] H. Li, M. Yang, J.S. Kim, J. Ha, J. Han, H. Kim, Y. Cho, J.Y. Wang, K.T. Nam, J. Yoon, Structure-oriented design strategy to construct NIR AIEgens to selectively combat gram (+) multidrug-resistant bacteria in vivo, Biomaterials 286 (2022), 121580.
[17] P. Manivasagan, J. Kim, E.S. Jang, Recent progress in multifunctional conjugated polymer nanomaterial- based synergistic combination phototherapy for microbial infection theranostics, Coord. Chem. Rev. 470 (2022), 214701.
[18] J. He, M. Hong, W.Q. Xie, Z. Chen, D.M. Chen, S.Y. Xie, Progress and prospects of nanomaterials against resistant bacteria, J. Contr. Release 351 (2022) 301–323.
[19] S. Chai, Y.T. Xie, L.H. Yang, Antibacterial applications of elemental nanomaterials, Curr. Opin. Solid St. M. 26 (6) (2022), 101043.
[20] Y.L. Hu, X.H. Ruan, X.Y. Lv, Y. Xu, W.J. Wang, Y. Cai, M. Ding, H. Dong, J.J. Shao, D.L. Yang, X.C. Dong, Biofilm microenvironment-responsive nanoparticles for the treatment of bacterial infection, Nano Today 46 (2022), 101602.
[21] X.Y. Lv, L.C. Wang, A.Q. Mei, Y. Xu, X.H. Ruan, W.J. Wang, J.J. Shao, D.L. Yang, X. C. Dong, Recent nanotechnologies to overcome the bacterial biofilm matrix barriers, Small 19 (6) (2022), 2206220.
[22] F.M. Lin, Z.H. Wang, F.G. Wu, Carbon dots for killing microorganisms: an update since, Pharmaceuticals 15 (10) (2019) 1236, 2022.
[23] Y.R. Chiou, C.J. Lin, S.G. Harroun, Y.R. Chen, L. Chang, A.T. Wu, F.C. Chang, Y. W. Lin, H.J. Lin, A. Anand, B. Unnikrishnan, A. Nain, C.C. Huang, Aminoglycoside-mimicking carbonized polymer dots for bacteremia treatment, Nanoscale 14 (32) (2022) 11719–11730.
[24] F.M. Lin, C.Y. Jia, F.G. Wu, Carbon dots for intracellular sensing, Small Struct. 3 (9) (2022), 2200033.
[25] B.Y. Wang, S.Y. Lu, The light of carbon dots: from mechanism to applications, Matter 5 (1) (2022) 110–149.
[26] B. Wang, H. Cai, G.I.N. Waterhouse, X. Qu, B. Yang, S. Lu, Carbon dots in bioimaging, biosensing and therapeutics: a comprehensive review, Small Science 2 (6) (2022), 2200012.
[27] M. Yu, X. Guo, H. Lu, P. Li, R. Huang, C. Xu, X. Gong, Y. Xiao, X. Xing, Carbon dots derived from folic acid as an ultra-succinct smart antimicrobial nanosystem for selective killing of S. aureus and biofilm eradication, Carbon 199 (2022) 395–406.
[28] M. Liu, L. Huang, X.Y. Xu, X.M. Wei, X.F. Yang, X.L. Li, B.N. Wang, Y. Xu, L.H. Li, Z. M. Yang, Copper doped carbon dots for addressing bacterial biofilm formation, wound infection, and tooth staining, ACS Nano 16 (6) (2022) 9479–9497.
[29] C.F. Zhao, X.W. Wang, L.N. Wu, W. Wu, Y.J. Zheng, L.Q. Lin, S.H. Weng, X.H. Lin, Nitrogen-doped carbon quantum dots as an antimicrobial agent against Staphylococcus for the treatment of infected wounds, Colloids Surf., B 179 (2019) 17–27.
[30] C.F. Zhao, X.W. Wang, L.Y. Yu, L.N. Wu, X.L. Hao, Q.C. Liu, L.Q. Lin, Z.J. Huang, Z. P. Ruan, S.H. Weng, A.L. Liu, X.H. Lin, Quaternized carbon quantum dots with broad-spectrum antibacterial activity for the treatment of wounds infected with mixed bacteria, Acta Biomater. 138 (2022) 528–544.
[31] W.B. Zhao, R.T. Wang, K.K. Liu, M.R. Du, Y. Wang, Y.Q. Wang, R. Zhou, Y.C. Liang, R.N. Ma, L.Z. Sui, Q. Lou, L. Hou, C.X. Shan, Near-infrared carbon nanodots for effective identification and inactivation of Gram-positive bacteria, Nano Res. 15 (3) (2021) 1699–1708.
[32] C. Mou, X. Wang, Y. Liu, Z. Xie, M. Zheng, Positively charged BODIPY@carbon dot nanocomposites for enhanced photomicrobicidal efficacy and wound healing, J. Mater. Chem. B 10 (39) (2022) 8094–8099.
[33] H. Wang, M. Zhang, Y. Ma, B. Wang, M. Shao, H. Huang, Y. Liu, Z. Kang, Selective inactivation of Gram-negative bacteria by carbon dots derived from natural biomass: artemisia argyi leaves, J. Mater. Chem. B 8 (13) (2020) 2666–2672.
[34] A. Pandey, A. Devkota, Z. Yadegari, K. Dumenyo, A. Taheri, Antibacterial properties of citric acid/beta-alanine carbon dots against gram-negative bacteria, Nanomaterials 11 (8) (2021), 2012.
[35] M. Varghese, M. Balachandran, Antibacterial efficiency of carbon dots against Gram-positive and Gram-negative bacteria: a review, J. Environ. Chem. Eng. 9 (6) (2021), 106821.
[36] P. Ezati, J.-W. Rhim, R. Molaei, R. Priyadarshi, S. Roy, S. Min, Y.H. Kim, S.-G. Lee, S. Han, Preparation and characterization of B, S, and N-doped glucose carbon dots: antibacterial, antifungal, and antioxidant activity, Sustain. Mater. Technol. 32 (2022), e00397.
[37] L. Wu, Y. Gao, C. Zhao, D. Huang, W. Chen, X. Lin, A. Liu, L. Lin, Synthesis of curcumin-quaternized carbon quantum dots with enhanced broad-spectrum antibacterial activity for promoting infected wound healing, Biomater. Adv. 133 (2022), 112608.
[38] L.N. Wu, Y.J. Yang, L.X. Huang, Y. Zhong, Y. Chen, Y.R. Gao, L.-Q. Lin, Y. Lei, A.-L. Liu, Levofloxacin-based carbon dots to enhance antibacterial activities and combat antibiotic resistance, Carbon 186 (2022) 452–464.
[39] L. Chen, C.F. Wang, C. Liu, S. Chen, Facile access to fabricate carbon dots and perspective of large-scale applications, Small (2022), e2206671.
[40] S. Zhu, X. Zhao, Y. Song, S. Lu, B. Yang, Beyond bottom-up carbon nanodots: citric-acid derived organic molecules, Nano Today 11 (2) (2016) 128–132.
[41] A.G. Grigoras, Natural and synthetic polymeric antimicrobials with quaternary ammonium moieties: a review, Environ. Chem. Lett. 19 (4) (2021) 3009–3022.
[42] S.H. Kim, D. Semenya, D. Castagnolo, Antimicrobial drugs bearing guanidine moieties: a review, Eur. J. Med. Chem. 216 (2021), 113293.
[43] X.L. Hao, L.L. Huang, C.F. Zhao, S.N. Chen, W.J. Lin, Y.N. Lin, L.R. Zhang, A. A. Sun, C.F. Miao, X.H. Lin, M. Chen, S.H. Weng, Antibacterial activity of positively charged carbon quantum dots without detectable resistance for wound healing with mixed bacteria infection, Mater. Sci. Eng. C Mater. Biol. Appl. 123 (2021), 111971.
[44] Q. Hu, Y. Fang, Z. Du, Z.L. Guo, Z.Y. Liu, Y. Huang, J. Lin, C.C. Tang, Controllable synthesis and enhanced microwave absorption properities of novel lightweight graphene quantum dots/hexagonal boron nitride composites, Carbon 182 (2021) 134–143.
[45] F.L. Zu, F.Y. Yan, Z.J. Bai, J.X. Xu, Y.Y. Wang, Y.C. Huang, X.G. Zhou, The quenching of the fluorescence of carbon dots: a review on mechanisms and applications, Microchim. Acta 184 (7) (2017) 1899–1914.
[46] H.J. Jian, R.S. Wu, T.Y. Lin, Y.J. Li, H.J. Lin, S.G. Harroun, J.Y. Lai, C.C. Huang, Super-cationic carbon quantum dots synthesized from spermidine as an eye drop formulation for topical treatment of bacterial keratitis, ACS Nano 11 (7) (2017) 6703–6716.
[47] Q.Q. Dou, X.T. Fang, S. Jiang, P.L. Chee, T.C. Lee, X.J. Loh, Multi-functional fluorescent carbon dots with antibacterial and gene delivery properties, RSC Adv. 5 (58) (2015) 46817–46822.
[48] J.J.Y. Zhang, Y. Chen, Synthesis and antimicrobial activity of polymeric guanidine and biguanidine salts, Polymer 40 (22) (1999) 6189–6198.
[49] Z.W. Jian, H. Wang, M.L. Liu, S.Y. Chen, Z.H. Wang, W. Qian, G.X. Luo, H.S. Xia, Polyurethane-modified graphene oxide composite bilayer wound dressing with long-lasting antibacterial effect, Mater. Sci. Eng. C Mater. Biol. Appl. 111 (2020), 110833.
[50] Q. Xu, B.F. Li, Y.C. Ye, W. Cai, W.J. Li, C.Y. Yang, Y.S. Chen, M. Xu, N. Li, X. S. Zheng, J. Street, Y. Luo, L.L. Cai, Synthesis, mechanical investigation, and application of nitrogen and phosphorus co-doped carbon dots with a high photoluminescent quantum yield, Nano Res. 11 (7) (2018) 3691–3701.
[51] S.J. Ye, D.F. Wei, X. Xu, Y. Guan, A. Zheng, Surface antimicrobial modification of polyamide by poly(hexamethylene guanidine) hydrochloride, Polym. Adv. Technol. 31 (8) (2020) 1847–1856.
[52] Y.W. Zhu, C. Xu, N. Zhang, X.K. Ding, B.R. Yu, F.J. Xu, Polycationic synergistic antibacterial agents with multiple functional components for efficient anti-infective therapy, Adv. Funct. Mater. 28 (14) (2018), 1706709.

[53] D. Gao, Y.S. Zhang, A.M. Liu, Y.D. Zhu, S.P. Chen, D. Wei, J. Sun, Z.Z. Guo, H. S. Fan, Photoluminescence-tunable carbon dots from synergy effect of sulfur doping and water engineering, Chem. Eng. J. 388 (2020), 124199.
[54] Y.L. Xu, B.Y. Wang, M.M. Zhang, J.X. Zhang, Y.D. Li, P.J. Jia, H. Zhang, L.L. Duan, Y. Li, Y.T. Li, X.L. Qu, S.H. Wang, D.H. Liu, W.P. Zhou, H.Z. Zhao, H.C. Zhang, L. X. Chen, X.L. An, S.Y. Lu, S.J. Zhang, Carbon dots as a potential therapeutic agent for the treatment of cancer-related anemia, Adv. Mater. 34 (19) (2022), 2200905.
[55] O. Ciofu, C. Moser, P.O. Jensen, N. Hoiby, Tolerance and resistance of microbial biofilms, Nat. Rev. Microbiol. 20 (10) (2022) 621–635.
[56] W.S. Hu, D.U. Woo, Y.J. Kang, O.K. Koo, Biofilm and spore formation of Clostridium perfringens and its resistance to disinfectant and oxidative stress, Antibiotics 10 (4) (2021) 396.
[57] X.Y. Li, D.M. Chen, S.Y. Xie, Current progress and prospects of organic nanoparticles against bacterial biofilm, Adv. Colloid. Interfac. 294 (2021), 102475.
[58] H.H. Ran, X. Cheng, Y.W. Bao, X.W. Hua, G. Gao, X. Zhang, Y.W. Jiang, Y.X. Zhu, F. G. Wu, Multifunctional quaternized carbon dots with enhanced biofilm penetration and eradication efficiencies, J. Mater. Chem. B 7 (33) (2019) 5104–5114.
[59] E. Sviridova, A. Barras, A. Addad, E. Plotnikov, A. Di Martino, D. Deresmes, K. Nikiforova, M. Trusova, S. Szunerits, O. Guselnikova, P. Postnikov, R. Boukherroub, Surface modification of carbon dots with tetraalkylammonium moieties for fine tuning their antibacterial activity, Biomater Adv 134 (2022), 112697.
[60] D. Zhao, R. Zhang, X.M. Liu, X.Y. Li, M.Y. Xu, X.J. Huang, X.C. Xiao, Screening of chitosan derivatives-carbon dots based on antibacterial activity and application in anti-Staphylococcus aureus biofilm, Int. J. Nanomed. 17 (2022) 937–952.
[61] P. Li, X. Yang, X. Zhang, J. Pan, W. Tang, W. Cao, J. Zhou, X. Gong, X. Xing, Surface chemistry-dependent antibacterial and antibiofilm activities of polyamine-functionalized carbon quantum dots, J. Mater. Sci. 55 (35) (2020) 16744–16757.
[62] W.F. Wu, Y.A. Qin, Y. Fang, Y.K. Zhang, S.X. Shao, F.X. Meng, M.W. Zhang, Based on multi-omics technology study the antibacterial mechanisms of pH-dependent N-GQDs beyond ROS, J. Hazard Mater. 441 (2023), 129954.
[63] D. Zhao, R. Zhang, X.M. Liu, X.Y. Li, M.Y. Xu, X.J. Huang, X.C. Xiao, Screening of chitosan derivatives-carbon dots based on antibacterial activity and application in anti-Staphylococcus aureus biofilm, Int. J. Nanomed. 17 (2022) 937–952.
[64] M.Q. Wang, Y.T. Su, Y.H. Liu, Y. Liang, S.S. Wu, N.L. Zhou, J. Shen, Antibacterial fluorescent nano-sized lanthanum-doped carbon quantum dot embedded polyvinyl alcohol for accelerated wound healing, J. Colloid Interface Sci. 608 (2022) 973–982.
[65] C.J. Mou, X.Y. Wang, J.H. Teng, Z.G. Xie, M. Zheng, Injectable self-healing hydrogel fabricated from antibacterial carbon dots and e-polylysine for promoting bacteria-infected wound healing, J. Nanobiotechnol. 20 (1) (2022) 368.
[66] Y. Imai, K.J. Meyer, A. Iinishi, Q. Favre-Godal, R. Green, S. Manuse, M. Caboni, M. Mori, S. Niles, M. Ghiglieri, C. Honrao, X.Y. Ma, J.J. Guo, A. Makriyannis, L. Linares-Otoya, N. Boehringer, Z.G. Wuisan, H. Kaur, R. Wu, A. Mateus, A. Typas, M.M. Savitski, J.L. Espinoza, A. O'Rourke, K.E. Nelson, S. Hiller, N. Noinaj, T. F. Schaberle, A. D'Onofrio, K. Lewis, A new antibiotic selectively kills Gram-negative pathogens, Nature 576 (7787) (2019) 459–464.
[67] D. Vejzovic, P. Piller, R.A. Cordfunke, J.W. Drijfhout, T. Eisenberg, K. Lohner, N. Malanovic, Where electrostatics matter: bacterial surface neutralization and membrane disruption by antimicrobial peptides SAAP-148 and OP-145, Biomolecules 12 (9) (2022) 1252.
[68] Y.L. Wang, Z.X. Li, D.J. Yang, X.Q. Qiu, Y.X. Xie, X. Zhang, Microwave-mediated fabrication of silver nanoparticles incorporated lignin-based composites with enhanced antibacterial activity via electrostatic capture effect, J. Colloid Interface Sci. 583 (2021) 80–88.
[69] M. Song, Y. Liu, X. Huang, S. Ding, Y. Wang, J. Shen, K. Zhu, A broad-spectrum antibiotic adjuvant reverses multidrug-resistant Gram-negative pathogens, Nat. Microbiol. 5 (8) (2020) 1040–1050.
[70] C.R. Raetz, C. Whitfield, Lipopolysaccharide endotoxins, Annu. Rev. Biochem. 71 (2002) 635–700.
[71] J.Y. Huang, F.L. Li, R.B. Guo, Y.Y. Chen, Z.Z. Wang, C.F. Zhao, Y.J. Zheng, S. H. Weng, X.H. Lin, A signal-on ratiometric fluorometric heparin assay based on the direct interaction between amino-modified carbon dots and DNA, Microchim. Acta 185 (5) (2018) 260.
[72] J.C. Xiao, X.L. Hao, C.F. Miao, F.L. Li, J.Y. Huang, X.H. Lin, M. Chen, X.W. Wu, S. H. Weng, Determination of chondroitin sulfate in synovial fluid and drug by ratiometric fluorescence strategy based on carbon dots quenched FAM-labeled ssDNA, Colloids Surf. B Biointerfaces 192 (2020), 111030.
[73] F.L. Li, Q.Q. Cai, X.L. Hao, C.F. Zhao, Z.J. Huang, Y.J. Zheng, X.H. Lin, S.H. Weng, Insight into the DNA adsorption on nitrogen-doped positive carbon dots, RSC Adv. 9 (22) (2019) 12462–12469.
[74] L. Wang, Z.C. Huang, Y.B. Liu, J. Wu, J.W. Liu, Fluorescent DNA probing nanoscale MnO(2): adsorption, dissolution by thiol, and nanozyme activity, Langmuir 34 (9) (2018) 3094–3101.
[75] Y.Q. Li, Z.J. Zhang, B.W. Liu, J.W. Liu, Adsorption of DNA oligonucleotides by boronic acid-functionalized hydrogel nanoparticles, Langmuir 35 (42) (2019) 13727–13734.
[76] C. Lu, Y.B. Liu, Y.B. Ying, J.W. Liu, Comparison of MoS_2, WS_2, and graphene oxide for DNA adsorption and sensing, Langmuir 33 (2) (2017) 630–637.
[77] P. Sondhi, M.H.U. Maruf, K.J. Stine, Nanomaterials for biosensing lipopolysaccharide, Biosensors 10 (1) (2019) 2.
[78] C. Lu, P.J.J. Huang, B.W. Liu, Y.B. Ying, J.W. Liu, Comparison of graphene oxide and reduced graphene oxide for DNA adsorption and sensing, Langmuir 32 (41) (2016) 10776–10783.
[79] J. Liu, Adsorption of DNA onto gold nanoparticles and graphene oxide: surface science and applications, Phys. Chem. Chem. Phys. 14 (30) (2012) 10485–10496.
[80] J.S. Park, H.K. Na, D.H. Min, D.E. Kim, Desorption of single-stranded nucleic acids from graphene oxide by disruption of hydrogen bonding, Analyst 138 (6) (2013) 1745–1749.
[81] Y. Chang, B. Liu, Z. Huang, Y. Liu, M. Liu, J. Liu, Yttrium oxide as a strongly adsorbing but nonquenching surface for DNA oligonucleotides, Langmuir 36 (4) (2020) 1034–1042.
[82] R. Kerr, S. Jabbari, J.M.A. Blair, I.G. Johnston, Dynamic Boolean modelling reveals the influence of energy supply on bacterial efflux pump expression, J. R. Soc., Interface 19 (186) (2022), 20210771.
[83] J. He, M. Hong, W.Q. Xie, Z. Chen, D.M. Chen, S.Y. Xie, Progress and prospects of nanomaterials against resistant bacteria, J. Contr. Release 351 (2022) 301–323.
[84] H.F. Wang, M.R. Chen, R.S. Tong, Z.J. Liu, Dosage regimen design of intravenous infusion administration of antimicrobial agents, China Pharmaceut. (2007) 1–3, 05.
[85] K. Kozics, M. Sramkova, K. Kopecka, P. Begerova, A. Manova, Z. Krivosikova, Z. Sevcikova, A. Liskova, E. Rollerova, T. Dubaj, V. Puntes, L. Wsolova, P. Simon, J. Tulinska, A. Gabelova, Pharmacokinetics, biodistribution, and biosafety of PEGylated gold nanoparticles in vivo, Nanomaterials 11 (7) (2021) 1702.
[86] J. Li, Z. Zhou, X. Liu, Y. Zheng, C. Li, Z. Cui, K.W.K. Yeung, H. Zhou, J. Zou, Z. Li, S. Zhu, Y. Liang, X. Wang, S. Wu, Material-herbology: an effective and safe strategy to eradicate lethal viral-bacterial pneumonia, Matter 4 (2021) 3030–3048.
[87] A.L. Bailly, F. Correard, A. Popov, G. Tselikov, F. Chaspoul, R. Appay, A. Al-Kattan, A.V. Kabashin, D. Braguer, M.A. Esteve, In vivo evaluation of safety, biodistribution and pharmacokinetics of laser-synthesized gold nanoparticles, Sci. Rep. 9 (2019), 12890.
[88] L. Velasquez-Garcia, A. Mejia-Sanjuanelo, D. Viasus, J. Carratala, Causative agents of ventilator-associated pneumonia and resistance to antibiotics in COVID-19 patients: a systematic review, Biomedicines 10 (6) (2022) 1226.
[89] F.Y. Wang, Z.C. Zuo, K.J. Chen, J. Fang, H.M. Cui, Y. Geng, P. Ouyang, Z.L. Chen, C. Huang, H.R. Guo, W.T. Liu, Diet-induced obesity mice execute pulmonary cell apoptosis via death receptor and ER-stress pathways after E. coli infection, Oxid. Med. Cell. Longev. 2020 (2020), 6829271.